NACA RM L58A10

7828

NACA

RESEARCH MEMORANDUM

EFFECTS OF NOSE AND AFTERBODY MODIFICATIONS ON

AERODYNAMIC CHARACTERISTICS OF A BODY WITH

AND WITHOUT A VERTICAL TAIL AT A

MACH NUMBER OF 2.01

By Gerald V. Foster

Langley Aeronautical Laboratory
Langley Field, Va.

NATIONAL ADVISORY COMMITTEE
FOR AERONAUTICS
WASHINGTON
April 15, 1958

NATIONAL ADVISORY COMMITTEE FOR AERONAUTICS

RESEARCH MEMORANDUM

EFFECTS OF NOSE AND AFTERBODY MODIFICATIONS ON

AERODYNAMIC CHARACTERISTICS OF A BODY WITH

AND WITHOUT A VERTICAL TAIL AT A
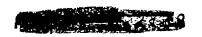
MACH NUMBER OF 2.01

By Gerald V. Foster

SUMMARY

The effects at a Mach number of 2.01 of various changes in nose and afterbody shape on the static aerodynamic characteristics of a body of revolution with a fineness ratio of 11 having an ogive nose, a cylindrical center section, and a boattail or cylindrical afterbody were investigated. The modified nose and afterbody had elliptical cross sections and could be orientated with the major axis of the cross section either vertical or horizontal. Some body configurations were tested in combination with a vertical tail.

The results show that positive increments of yawing moment were provided by the vertical elliptic afterbody through the angle-of-attack range and by the horizontal elliptic nose at large angles of sideslip and large angles of attack. The vertical elliptic afterbody had no significant effect on the vertical-tail contribution to directional stability; whereas, the horizontal elliptic nose increased the directional-stability contribution of the vertical tail in the presence of the vertical elliptic afterbody at low and moderate angles of attack but had an adverse effect at high angles of attack. The horizontal elliptic afterbody provided negative increments of pitching moment but had no appreciable effect on the directional stability of the body. The vertical elliptic nose adversely affected the directional stability of the body.

INTRODUCTION

The static directional stability of many current high-speed-airplane configurations becomes marginal at undesirably low angles of attack at low supersonic Mach numbers. This condition is associated with a decrease

in vertical-tail effectiveness and the inherent instability of wing-body configurations having high-fineness-ratio bodies with a far rearward center of gravity (refs. 1 and 2). In some cases the directional stability has been improved by an increase in vertical-fin area. (For example, see refs. 3 and 4.) Another approach to the problem of obtaining directional stability has been the use of small horizontal fins on the body nose which improved the directional stability of the wing-body configuration and thus improved the directional stability of the wing-body-tail configuration. (See ref. 5.)

An investigation has been conducted to determine if the contribution of a body of revolution to directional stability of an airplane configuration could be improved by flattening either the nose, the afterbody, or both. The modified nose had elliptic cross sections in both the vertical and horizontal plane, with the volume equal to that of the basic ogive nose. The modified afterbody had elliptic cross sections, the cross-sectional area of which was equal to that of the cylindrical section of the body.

The results presented herein show the effects of various arrangements of these modifications on both the longitudinal and the lateral aerodynamic characteristics of the body configuration alone and in combination with a vertical tail. These data were obtained at a Mach number of 2.01 through a range of sideslip angle from 0° to 20° (unless restricted by mechanical limitations) at various angles of attack from 0° to about 25°.

SYMBOLS

The forces and moments for the various body configurations are presented in coefficient form. The coefficients have been based on the dimensions of a wing given in reference 6. The data are referred to the body axis with the origin located at a point 57 percent body length from the nose, which corresponds to a wing quarter-chord location on a body reported in reference 6. The symbols used herein are defined as follows:

C_N　　　normal-force coefficient, F_N/qS

C_A　　　chord-force coefficient, F_A/qS

C_m　　　pitching-moment coefficient, $M_Y/qS\bar{c}$

C_n　　　yawing-moment coefficient, M_Z/qSb

C_l rolling-moment coefficient, M_X/qSb

C_Y side-force coefficient, F_Y/qS

F_N normal force

F_A chordwise force

F_Y side force

M_Y pitching moment

M_Z yawing moment

M_X rolling moment

q free-stream dynamic pressure, lb/sq ft

S wing area, sq ft

b wing span, ft

$\bar{c}$ mean geometric chord, in.

β angle of sideslip, deg

α angle of attack, deg

C_{n_β} directional-stability parameter

C_{l_β} rolling-moment parameter

C_{Y_β} side-force parameter

r radius, in.

x longitudinal distance along fuselage center line, in.

C coordinate along major axis of elliptic nose, in.

D coordinate along minor axis of elliptic nose, in.

A coordinate along major axis of elliptic afterbody, in.

B   coordinate along minor axis of elliptic afterbody, in.

Model notation:

N_V elliptic nose with major axis vertical

N_H elliptic nose with major axis horizontal

A_V elliptic afterbody with major axis vertical

A_H elliptic afterbody with major axis horizontal

A_B boattail afterbody

A_C cylindrical afterbody

MODEL AND APPARATUS

The bodies used in this investigation had either an ogive or an elliptic nose, a cylindrical center section, and a boattail, a cylindrical, or an elliptic afterbody. Coordinates of the body having an ogive nose and boattail afterbody are presented in table I. Details of the elliptic nose and elliptic afterbody are presented in figure 1(a) and tables II and III. The elliptic nose was designed so that the cross-sectional area at a given body station is equivalent to the cross-sectional area of the ogive nose. The cross-sectional area of the elliptic after-body is equal to the cross-sectional area of the cylindrical afterbody and is constant along the afterbody length. Both the elliptic nose and the afterbody could be orientated with the cross-sectional major axis either vertical or horizontal. The ratio of the side area of the ellip-tic nose with the cross-sectional major axis horizontal and vertical to the projected area of the ogive nose was 0.71 and 1.47, respectively. The ratio of the side area of the elliptic afterbody with the cross-sectional major axis horizontal and vertical to the projected area of the boattailed afterbody was 0.90 and 1.60, respectively. The ratio of the projected area of the boattail afterbody to that of the cylindrical afterbody was 0.92. The ratio of length to diameter of the bodies was approximately 11.

The side area of the elliptic afterbody with the cross-sectional major axis vertical was simulated by two fins made of sheet metal and attached to the cylindrical afterbody. (See fig. 1(b).)

The elliptic afterbody was designed so that a vertical tail could be installed in the plane of the major axis. The vertical tail used with this afterbody had a taper ratio of 0.20 and an aspect ratio of 1.75 (if it is assumed that the tail extended to the center line of the body). The vertical tail used with the cylindrical afterbody was identical in plan form with the one used with the elliptic afterbody (fig. 2), but because of differences in afterbodies, the exposed tail area in this case was 25 percent greater than that with the elliptic afterbody.

TESTS, CORRECTIONS, AND ACCURACY

The tests were conducted in the Langley 4- by 4-foot supersonic pressure tunnel with the models mounted on a six-component balance attached to a rotary-type sting. This mounting permitted measurement of six-component data through a sideslip range from 0° to 28° (unless restricted because of mechanical limitations) at angles of attack of approximately 0°, 4°, 8°, 12°, 16°, 20°, and 24°. The various body configurations investigated are shown in figure 3. The test conditions are as follows:

Mach number 2.01
Stagnation pressure, lb/sq in. abs 10.0
Stagnation temperature, $^\circ$F 100.0
Reynolds number, based on $\bar{c} = 6.89$ in. . . . . 1.42 $\times 10^6$

The stagnation dewpoint was maintained sufficiently low (-25° F or less) so that no condensation effects were encountered in the test section.

The values of angle of attack and sideslip have been corrected for sting deflection due to load. The base pressure was measured, and the drag force was adjusted to a base pressure equal to the free-stream static pressure.

The estimated errors in the individual measured quantities are as follows:

C_N . . . . ±0.0113
C_A . . . . ±0.0009
C_m . . . . ±0.0003
C_n . . . . ±0.0004
C_l . . . . ±0.0003
C_y . . . . ±0.001

PRESENTATION OF RESULTS

The data presented in figures 4 to 7 include the aerodynamic characteristics of various body configurations investigated. A comparison of the lateral aerodynamic characteristics of the boattail and cylindrical afterbody configurations is presented in figure 8. Figure 9 shows a comparison of the effects of afterbody fins and vertical elliptic afterbody on the directional-stability characteristics. Figure 10 presents schlieren photographs of various body configurations. Results obtained with various body configurations with a vertical tail are presented in figures 11 to 13. Figures 14 to 16 summarize the effect of various body modifications on the directional-stability characteristics ($\beta = 0^\circ$) of body alone and body—vertical-tail combinations.

DISCUSSION

Effects of Nose and Afterbody Modifications

In general, the boattail body exhibited fairly linear variations of C_n with β (fig. 4) which averaged approximately -0.0018 through the angle-of-attack range investigated (see fig. 14). Figure 4 indicates that a change in nose shape from ogival to elliptical had an adverse effect on the directional stability throughout the angle-of-attack range when the cross-sectional axis was vertical; whereas, favorable changes in yawing moment were obtained with the cross-sectional major axis horizontal. At $\alpha = 0^\circ$ the horizontal elliptic nose had no significant effect on the yawing moment at angles of sideslip below 8°; however, at large angles of sideslip this modification N_H provided a large positive incremental change in yawing moment. With an increase in angle of attack the initial stabilizing change in yawing moment of N_H occurred at progressively lower angles of sideslip, and an approximately linear variation of C_n with β at angles of attack 20.5° and 24.6° resulted. These changes in directional stability of the horizontal elliptic nose configuration were accompanied by destabilizing changes in pitching moment which became progressively larger with an increase in angle of attack. The changes in the directional characteristic of N_H at $\alpha = 0^\circ$ might be associated with a rearward shift of the lateral center of pressure, possibly because of the effect of a change in body crossflow in the region of the nose. When the decrease in side area of N_H is considered, the rearward shift of the lateral center of pressure might be associated with a decrease in side force along the nose; however, it may be noted in figure 4 that the total side force accompanying the initial change in yawing moment was not significantly affected by N_H.
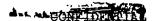
With an increase in angle of attack the nose developed a positive lift increment resulting in an unstable pitching-moment increment while concurrent changes in directional stability were associated primarily with a rearward shift of the lateral center of pressure, although the cause is not readily apparent.

The results showing the effect on the aerodynamic characteristics of changes in afterbody from boattail to elliptic are presented in figure 5. As would be expected, with an increase in side area aft of the center of gravity, the vertical elliptic afterbody A_V provided an increase in negative side force accompanied by a decrease in negative yawing moment for all values of α and β investigated (also, see fig. 14). The pitching-moment characteristics of A_V were essentially the same as for the boattail configuration. The horizontal elliptic afterbody configuration, when compared with the boattail configuration, provided a stabilizing change in pitching moment but had only a small effect on the directional-stability characteristics. In order to determine if the effect of A_V is derived solely from an increase in side area, afterbody fins were attached in a vertical plane to the cylindrical configuration. The projected side area of this configuration was identical to the A_V configuration. The data presented in figure 9 indicate that at angles of attack of $0°$ and $4°$ both afterbody fins and the vertical elliptic afterbody provided an increase in side force and a decrease in yawing moment of approximately the same order. At higher angles of attack the afterbody fins, in contrast to A_V, were not effective near $\beta = 0°$; whereas, at moderate angles of sideslip the fins appear to have resulted in a small increase in negative side force and a small decrease in negative yawing moment.

The combined effects of nose and afterbody modifications on the aerodynamic characteristics are presented in figures 6 and 7. In general, these data indicate the directional stability of the elliptic afterbody configuration increased with N_H (fig. 6) and decreased with N_V (fig. 7). The changes in directional stability of the body with N_H were greater with A_V than with A_H (fig. 6) except for large angles of attack at low angles of sideslip. (See fig. 14, for example.) The effect of the nose modification N_H in conjunction with A_V resulted in a decrease in C_{n_β} at low angles of attack which increased in magnitude with an increase in angle of attack up to $14°$ (fig. 14). At angles of attack greater than $18°$ the $N_H A_V$ configuration exhibits more positive values of C_{n_β} than the body with an ogive nose and vertical elliptic afterbody. This comparison was limited to a small range of sideslip angles near $\beta = 0°$ because of the nonlinearity of C_n at moderate and large angles of sideslip. The change in C_n for large sideslip angles

of the body with $N_H A_V$ was of a stabilizing nature, as in the case of
the body with N_H and boattail afterbody, but was appreciably larger
in magnitude. It would appear that these changes in the directional
stability of $N_H A_V$ might prevent digressions to large sideslip angles.
The changes in the pitching-moment characteristics caused by N_H were
not appreciably altered by changing the afterbody from the boattail
afterbody to the vertical elliptic afterbody.

Vertical Tail-On Configurations

Results for the configurations with the tail on the cylindrical
body or the vertical elliptic afterbody, in combination with either the
ogive nose or the horizontal elliptic nose, are presented in figures 11,
12, and 13. The data for the tail-off configurations were included in
these figures for comparison purposes. The yawing-moment results of
the body-tail configurations investigated were essentially linear with
sideslip angle up to an angle of attack of approximately 12°, and above
an angle of attack of 12° the yawing moments varied nonlinearly with
sideslip angle (see figs. 11 to 13). A comparison of the effects of
various modifications on C_{n_β} (fig. 16) for angles of attack up to
approximately 12° indicates that, although the directional stability of
all tail-on configurations decreased gradually with an increase in angle
of attack, both modified bodies $\left(A_V \text{ and } N_H A_V\right)$ exhibited a substantial
improvement in the directional stability. For example, at $\alpha = 0°$ a
change in afterbody configuration from cylindrical to A_V resulted in
an increase in C_{n_β} from 0.0006 to 0.0015; whereas, the improvement
obtained with $N_H A_V$ was approximately 50 percent greater than with A_V.
The stability parameters presented in figure 16 for angles of attack
greater than approximately 12° are restricted to a range of sideslip
angle of 2° because of nonlinearity of the yawing-moment characteristics.
At high angles of attack figure 16 tends to indicate that although all
tail-on configurations became directionally unstable, the modified after-
body configuration A_V exhibited less negative directional stability
than the cylindrical afterbody; whereas, the directional stability of
the modified-nose—afterbody configuration when compared with the cylin-
drical afterbody configuration is more negative. It may be seen by com-
paring the yawing-moment characteristics (figs. 12 and 13) that the
directional stability of the modified-nose—afterbody configuration
$N_H A_V$ at high angles of attack and sideslip angle greater than 2° is
more positive than the modified afterbody configuration A_V.

Some insight as to the effect of these modifications can be gained
from an examination of the tail contribution. Comparison of the

yawing-moment characteristics of the tail-on and tail-off configurations (figs. 11 and 12) indicates a decrease in vertical-tail contribution with the modified afterbody configuration A_V. This decrease is associated primarily with the decrease in exposed tail area incurred with the vertical elliptic afterbody. The increase in directional stability with the modified body N_HA_V relative to the modified afterbody configuration A_V was caused by an increase in vertical-tail contribution (figs. 12 and 13) which might be associated with a favorable flow disturbance emanating from the nose. At high angles of attack the N_V had an adverse effect on the directional-stability contribution of the vertical tail in the presence of A_V.

CONCLUSIONS

An investigation conducted at a Mach number of 2.01 to determine the effects of a change in cross-sectional shape of the nose and afterbody from circular to elliptic on the aerodynamic characteristics of a body indicate that:

1. The vertical elliptic afterbody improved the directional stability of the body alone through the angle-of-attack range and had no significant effect on the vertical-tail contribution to the directional stability.

2. The horizontal elliptic nose provided positive increments of yawing moment at large angles of sideslip and large angles of attack accompanied by positive increments of pitching moment. This nose configuration increased the directional-stability contributions of the vertical tail in the presence of the vertical elliptic afterbody at low and moderate angles of attack but had an adverse effect at high angles of attack.

3. The horizontal elliptic afterbody provided negative increments of pitching moment, but had no appreciable effect on the directional stability of the body.

4. The vertical elliptic nose adversely affected the directional stability of the body.

Langley Aeronautical Laboratory,
National Advisory Committee for Aeronautics,
Langley Field, Va., December 16, 1957.

　　　　　　　　　　　　　　　　　　NACA RM L58A10

REFERENCES

1. Polhamus, Edward C., and Hallissy, Joseph M., Jr.: Effect of Airplane
   Configuration on Static Stability at Subsonic and Transonic Speeds.
   NACA RM L56A09a, 1956.

2. Spearman, M. Leroy, and Henderson, Arthur, Jr.: Some Effects of Air-
   craft Configuration on Static Longitudinal and Directional Stability
   Characteristics at Supersonic Mach Numbers Below 3. NACA RM L55L15a,
   1956.

3. Spearman, M. Leroy, and Robinson, Ross B.: Static Lateral Stability
   and Control Characteristics of a Model of a 45° Swept-Wing Fighter
   Airplane With Various Vertical Tails at Mach Numbers of 1.41, 1.61,
   and 2.01. NACA RM L56D05, 1956.

4. Spearman, M. Leroy: Some Factors Affecting the Static Longitudinal
   and Directional Stability Characteristics of Supersonic Aircraft
   Configurations. NACA RM L57E24a, 1957.

5. Sleeman, William C., Jr.: Investigation at High Subsonic Speeds of
   the Effects of Various Horizontal Fuselage Forebody Fins on the
   Directional and Longitudinal Stability of a Complete Model Having
   a 45° Sweptback Wing. NACA RM L56J25, 1957.

6. Spearman, M. Leroy: Investigation of the Aerodynamic Characteristics
   in Pitch and Sideslip of a 45° Sweptback-Wing Airplane Model With
   Various Vertical Locations of the Wing and Horizontal Tail - Effect
   of Wing Location and Geometric Dihedral for the Wing-Body Combination,
   M = 2.01. NACA RM L55B18, 1955.

TABLE I.- COORDINATES OF BODY OF REVOLUTION

x, in.	r, in.
0	0
2.00	.53
4.00	.96
6.00	1.28
8.00	1.51
10.00	1.63
11.67	1.67
28.56	1.67
36.64	1.38

TABLE II.- ELLIPTIC NOSE COORDINATES
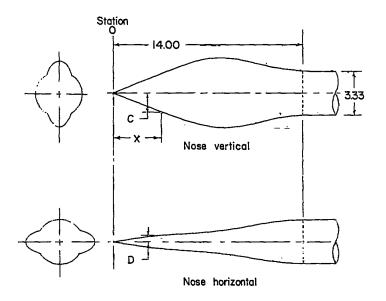
x, in.	C, in.	D, in.
0	0	0
1.00	.44	.17
2.00	.87	.32
3.00	1.26	.45
4.00	1.66	.55
5.00	2.04	.62
6.00	2.41	.68
7.00	2.64	.75
8.00	2.64	.86
9.00	2.45	1.02
10.00	2.19	1.22
11.00	1.95	1.41
12.00	1.79	1.55
13.00	1.70	1.64
14.00	1.68	1.68

TABLE III.- ELLIPTIC AFTERBODY COORDINATES

x, in.	A, in.	B, in.
27.75	1.67	1.67
28.50	1.70	1.63
29.25	1.79	1.55
30.00	1.95	1.43
30.75	2.16	1.28
31.50	2.36	1.18
32.25	2.45	1.13
33.00	2.49	1.12
33.50	2.50	1.11
36.64	2.50	1.11
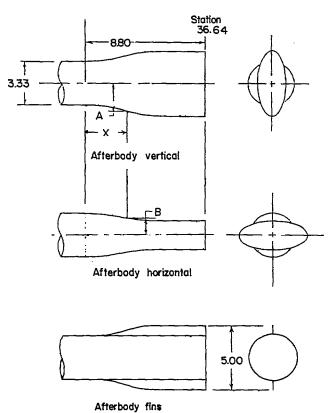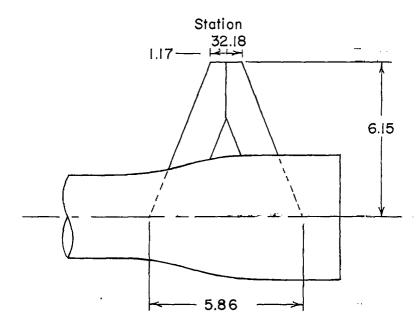
Figure 1.- Details of elliptic nose and elliptic afterbody. All dimensions are in inches.

Station
32.18

1.17

6.15

5.86

Station
32.18

1.17

6.15

5.86
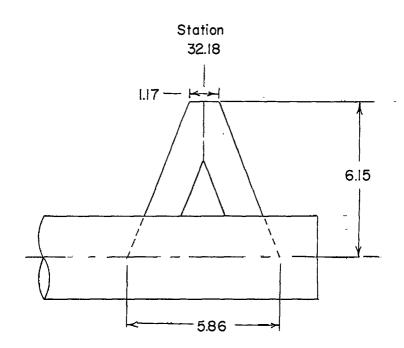
Figure 2.- Schematic view of vertical tail. All dimensions are in inches.
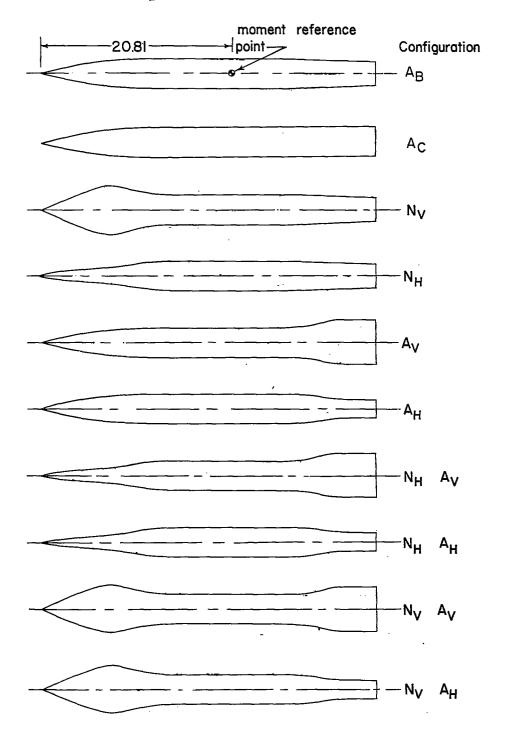
Figure 3.- Side veiw of various body configurations. All dimensions are in inches.

(a) $\alpha = 0°$.
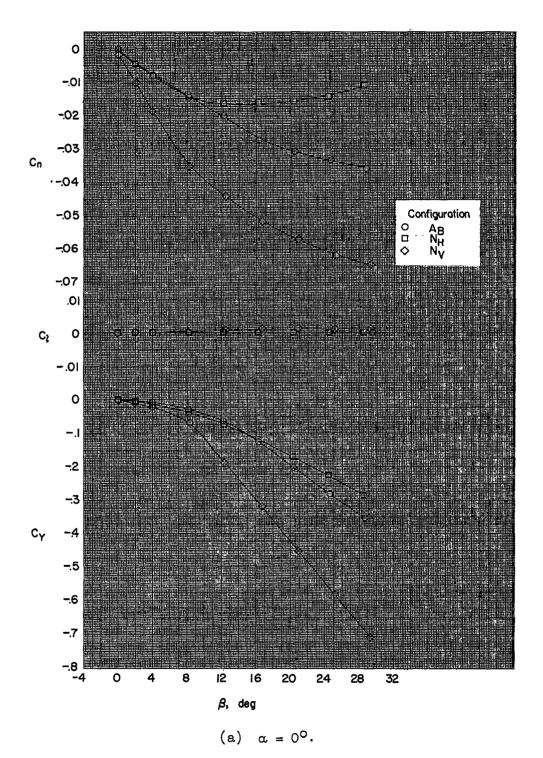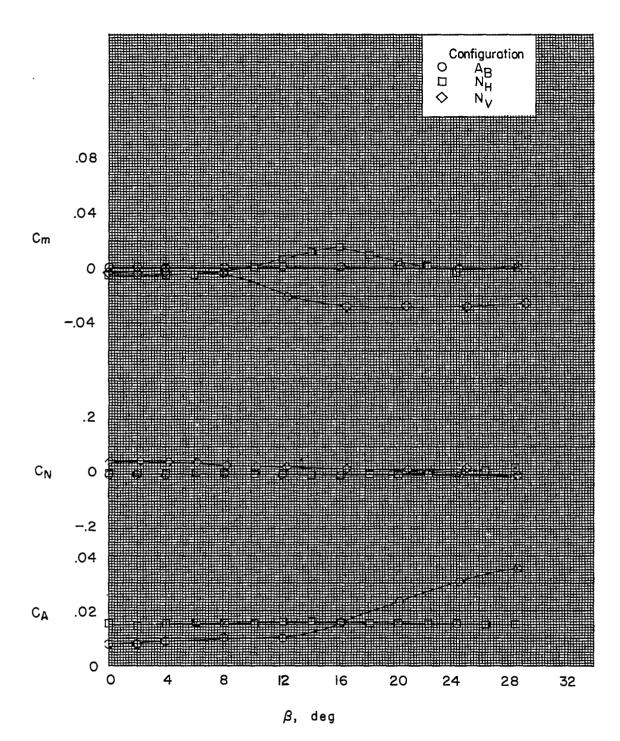
Figure 4.- Aerodynamic characteristics in sideslip of a body with various nose configurations.
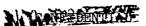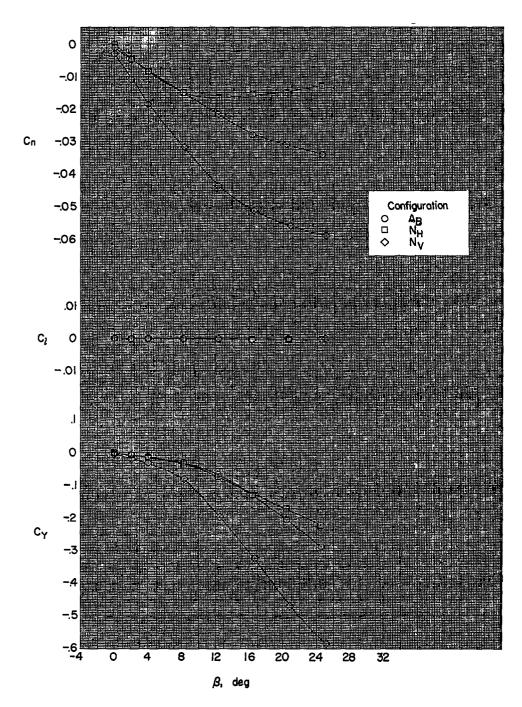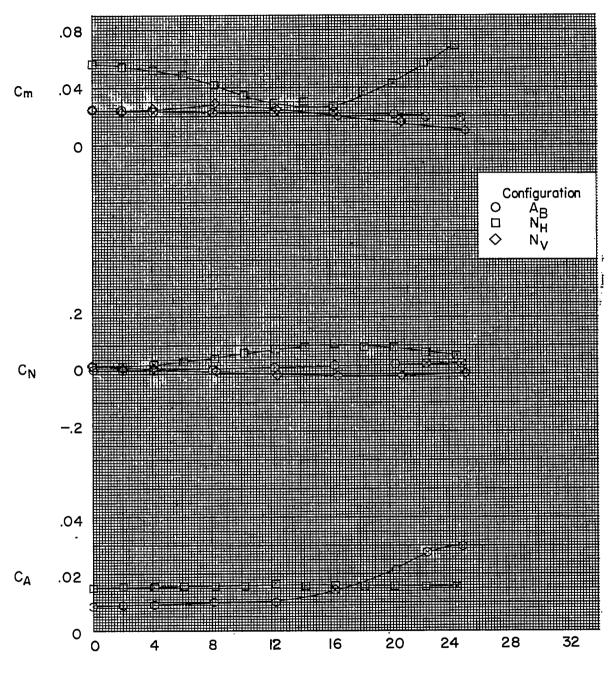
(a) Concluded.

Figure 4.- Continued.

(b) $\alpha = 4.1^{\circ}$.

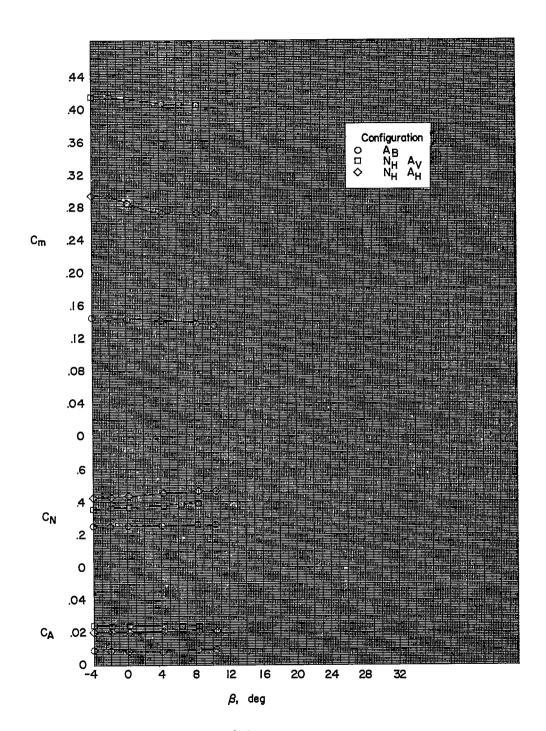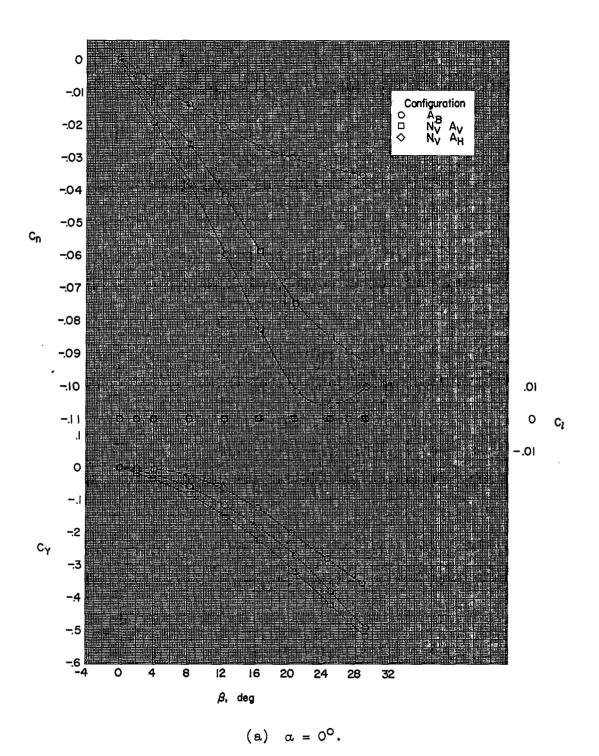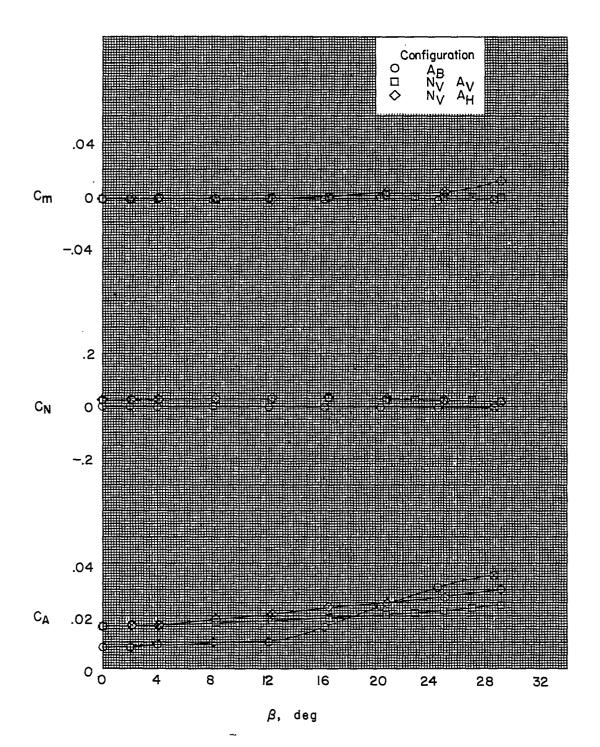Figure 4.- Continued.

(b) Concluded.

Figure 4.- Continued.

(c) α = 8.2°.

Figure 4.- Continued.

Configuration

O	A_B
□	N_H
◇	N_V

β, deg
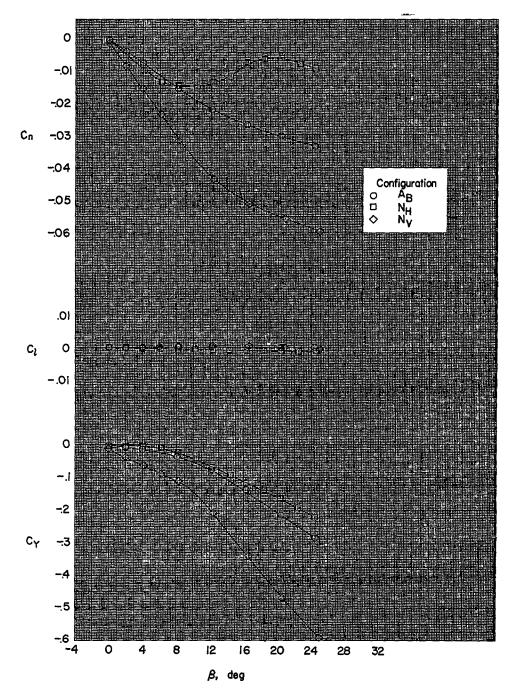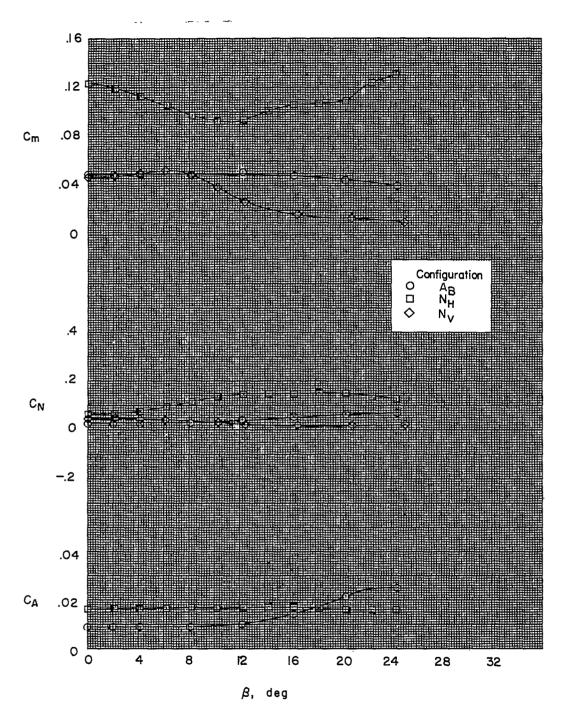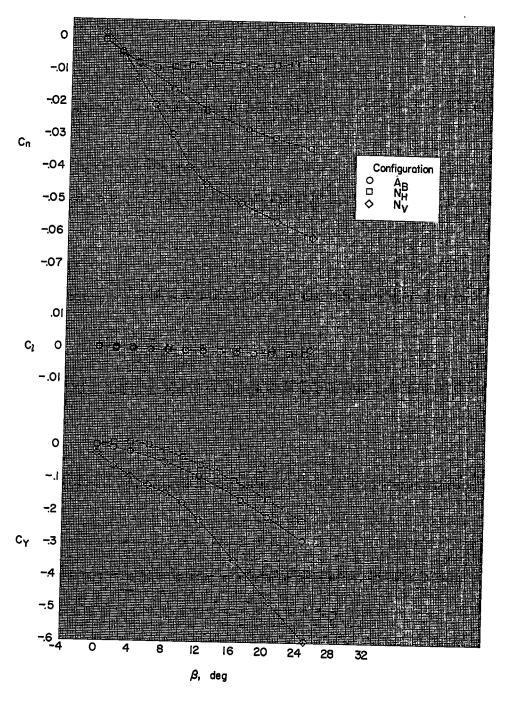
(c) Concluded.
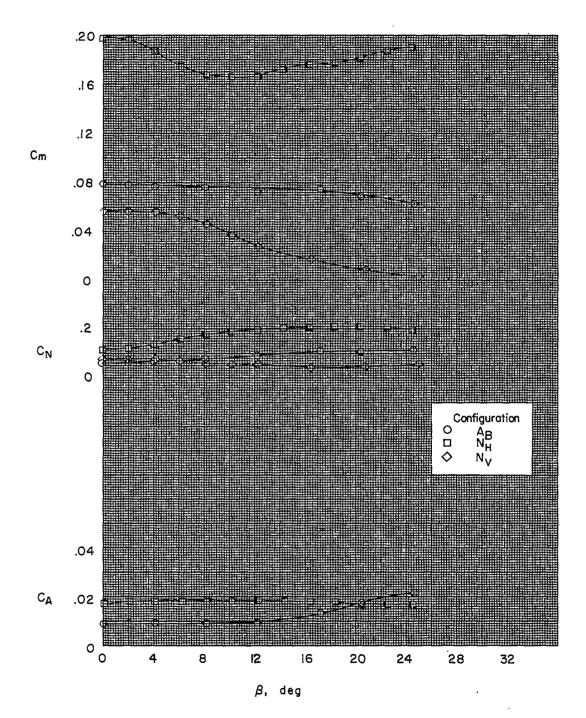
Figure 4.- Continued.

(d) $\alpha = 12.3^{\circ}$.

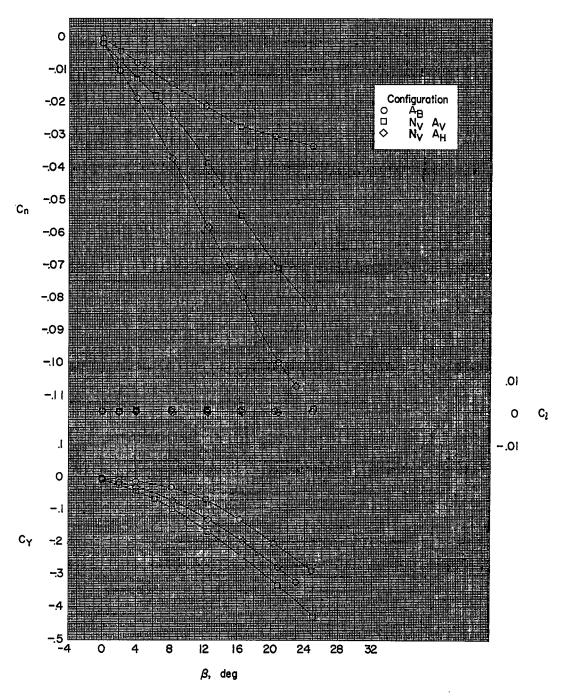Figure 4.- Continued.
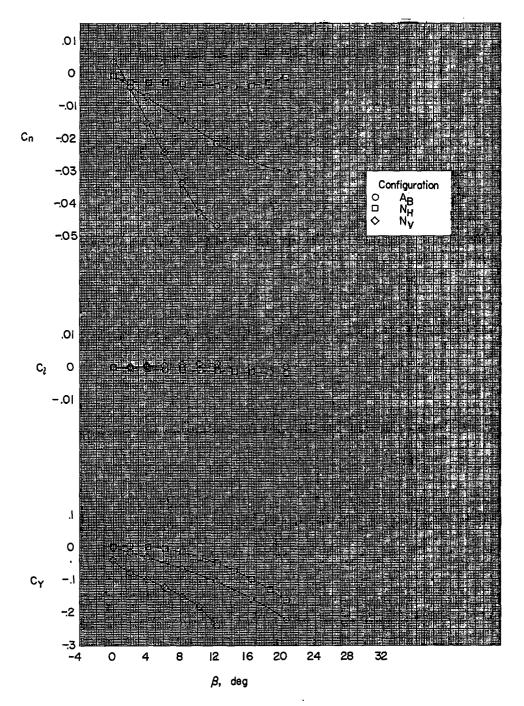
(d) Concluded.
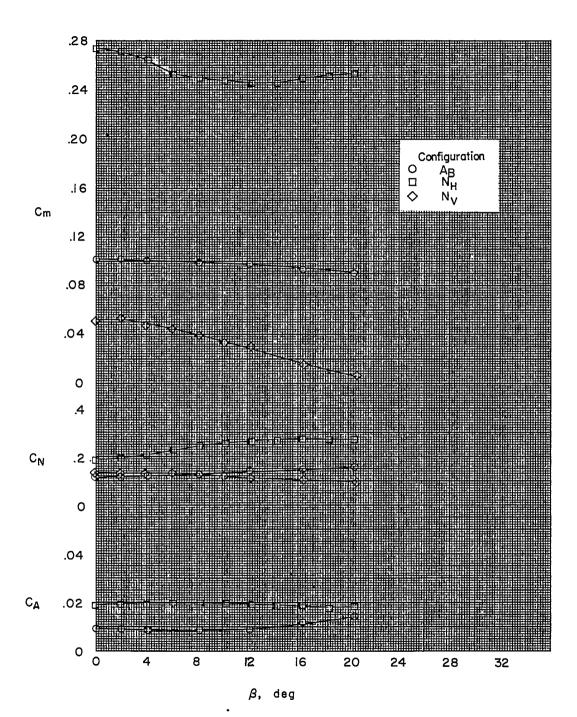
Figure 4.- Continued.

(e) $\alpha = 16.4^{\circ}$.

Figure 4.- Continued.
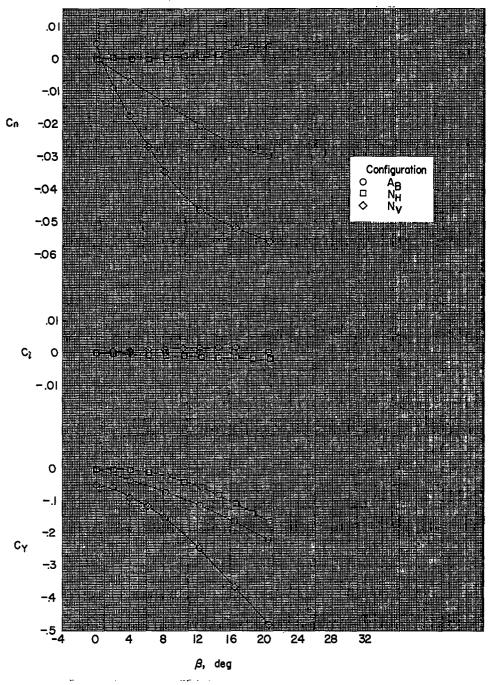
(e) Concluded.
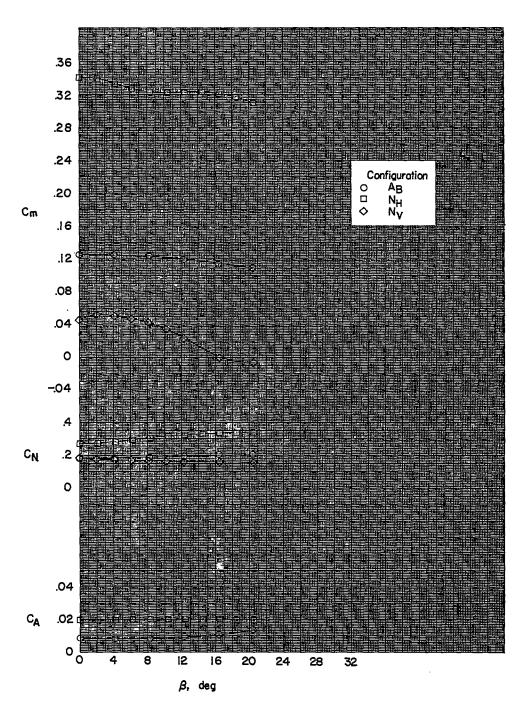
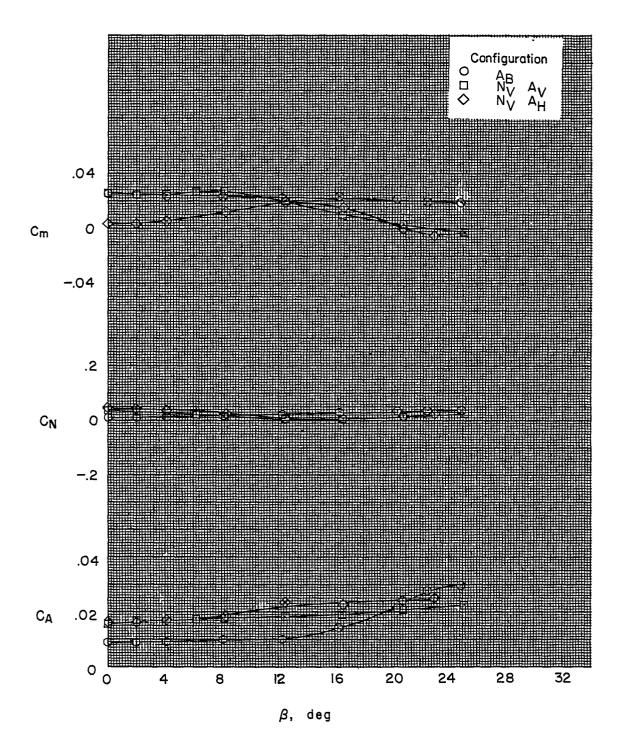Figure 4.- Continued.

(f) $\alpha = 20.5^{\circ}$.
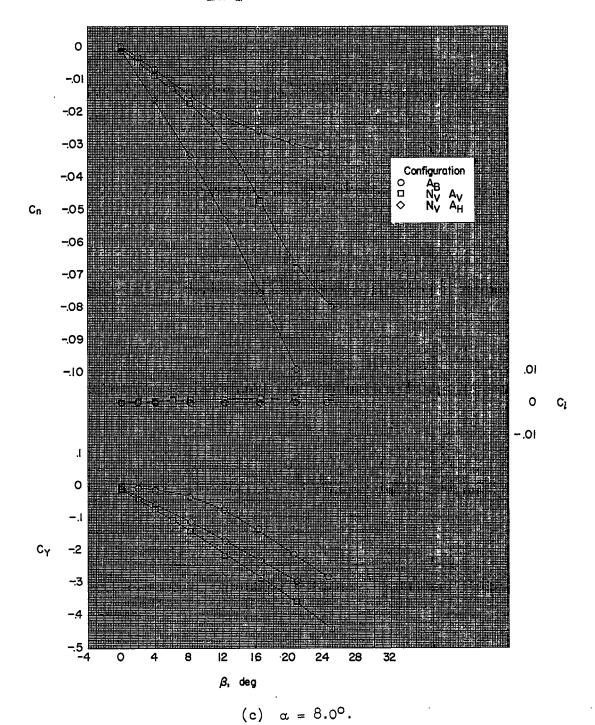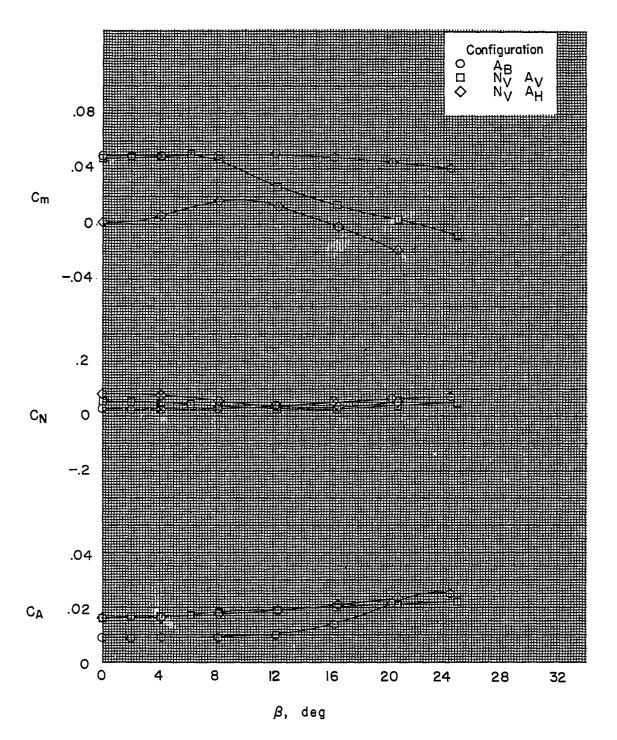
Figure 4.- Continued.
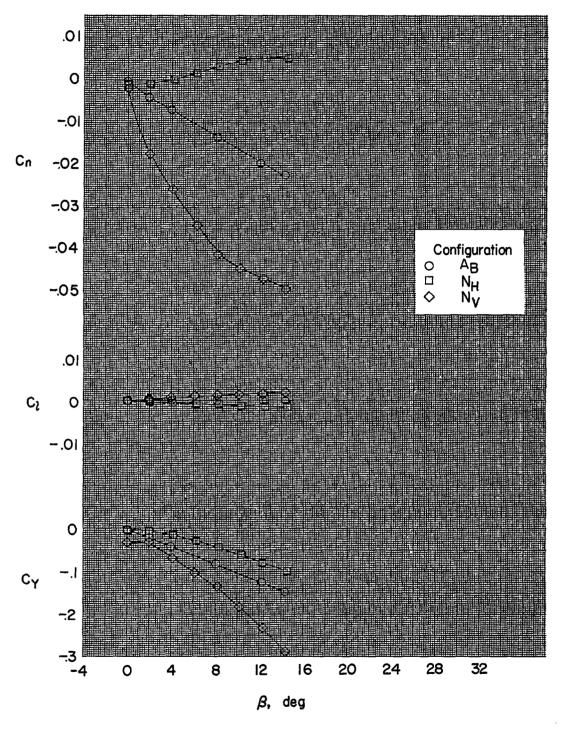
(f) Concluded.
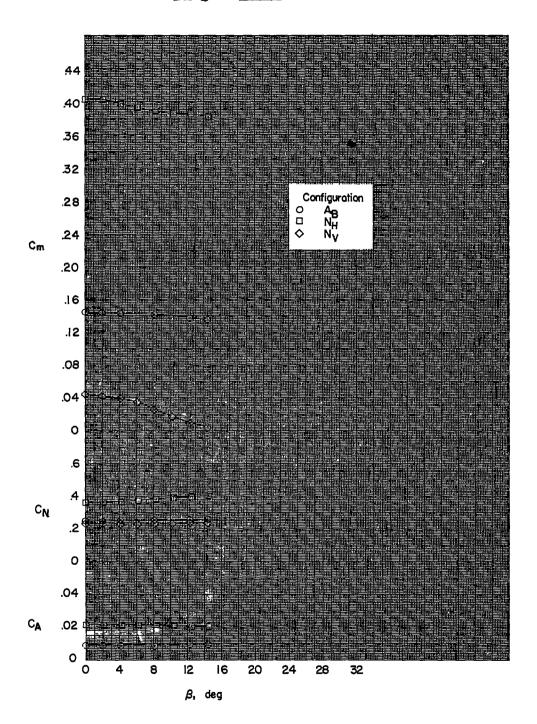
Figure 4.- Continued.

(g) $\alpha = 24.6^{\circ}$.

Figure 4.- Continued.

(g) Concluded.

Figure 4.- Concluded.

(a) $\alpha = 0°$.
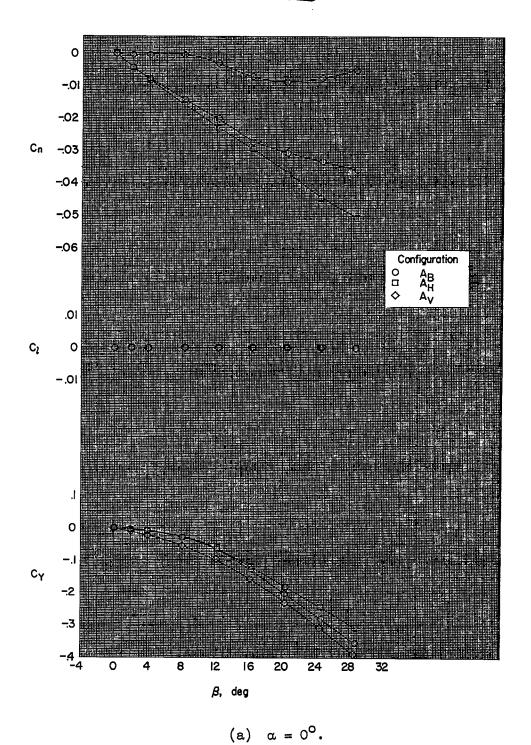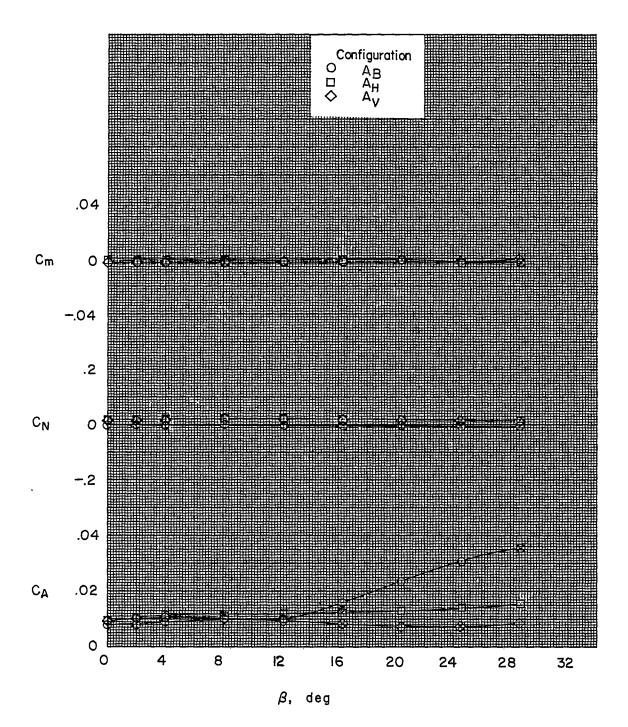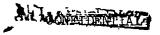
Figure 5.- Aerodynamic characteristics of a body in sideslip with various afterbody configurations.
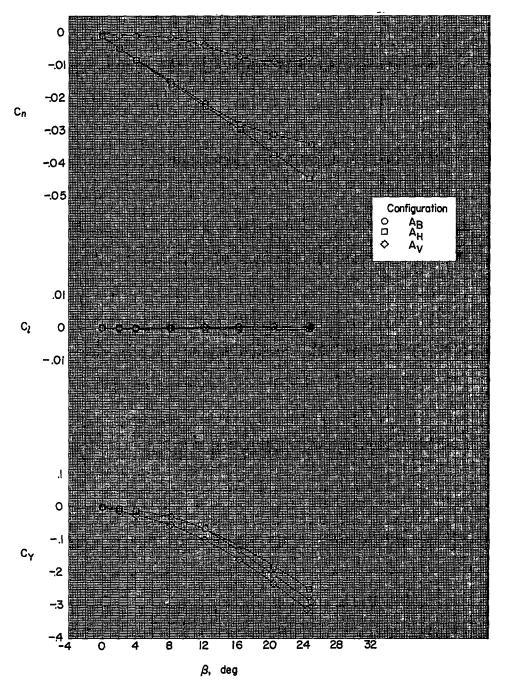
(a) Concluded.
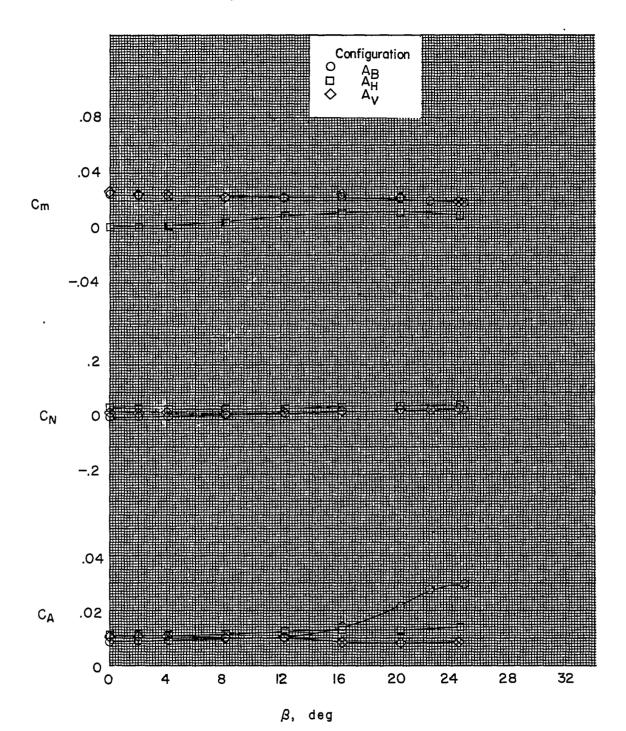
Figure 5.- Continued.

(b) $\alpha = 4.1^\circ$.

Figure 5.- Continued.
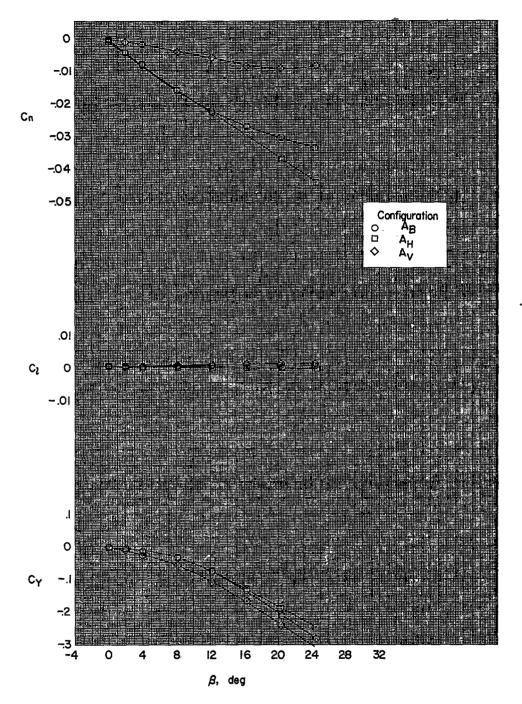
S

(b) Concluded.
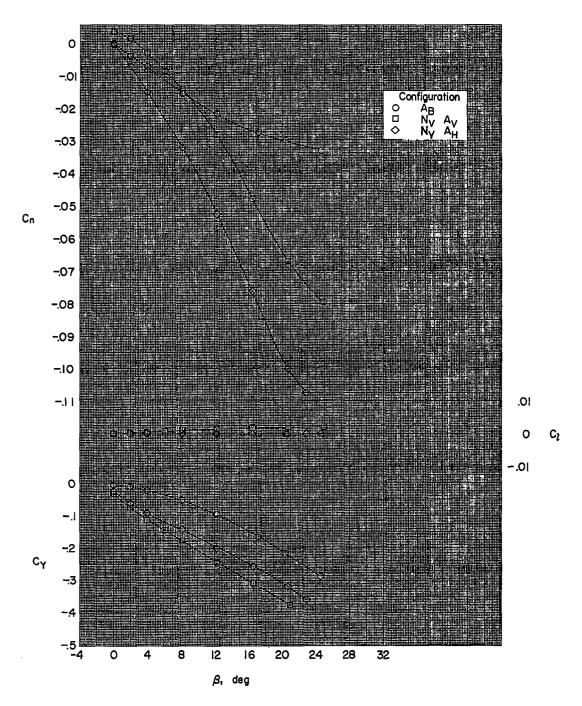
Figure 5.- Continued.
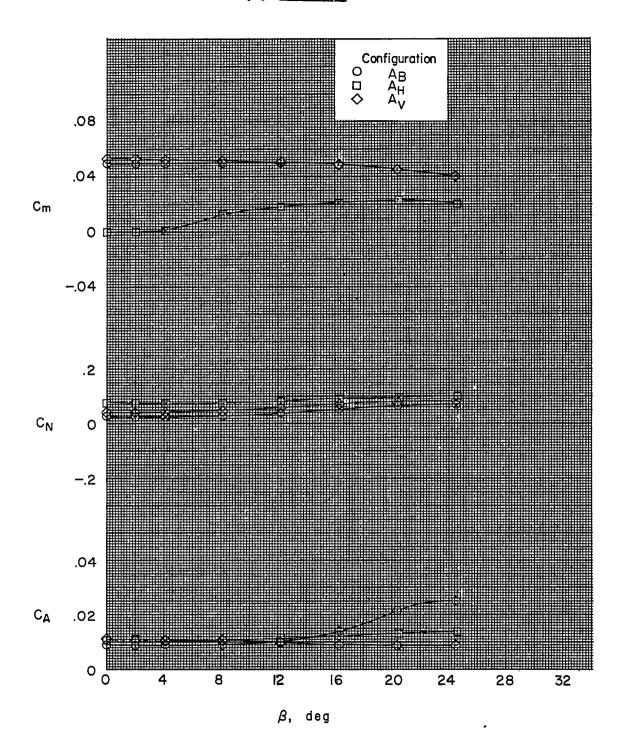
(c) $\alpha = 8.2^{\circ}$.

Figure 5.- Continued.
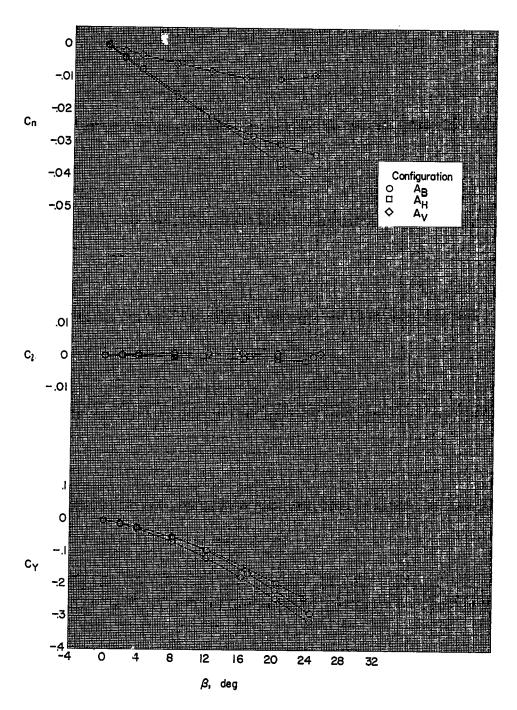
(c) Concluded.
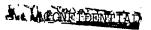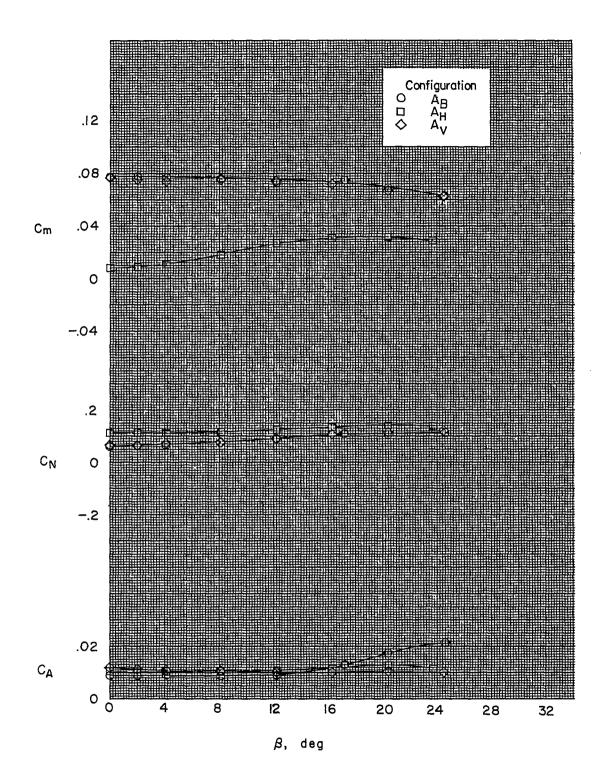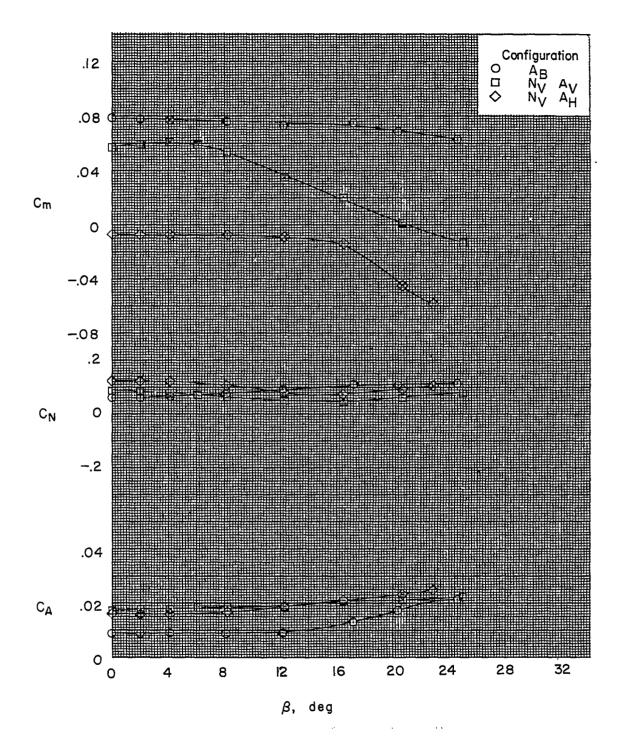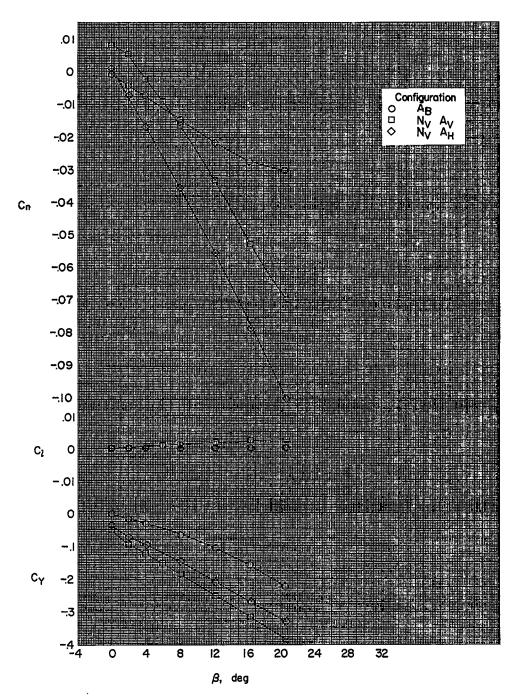
Figure 5.- Continued.

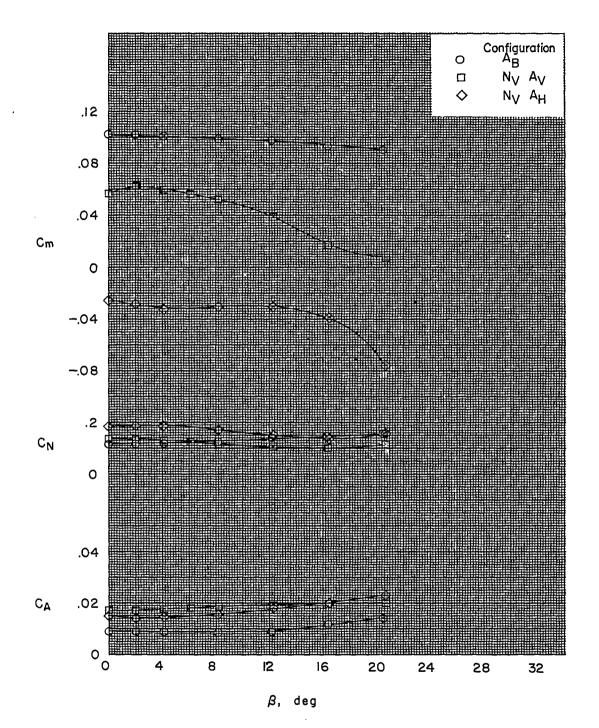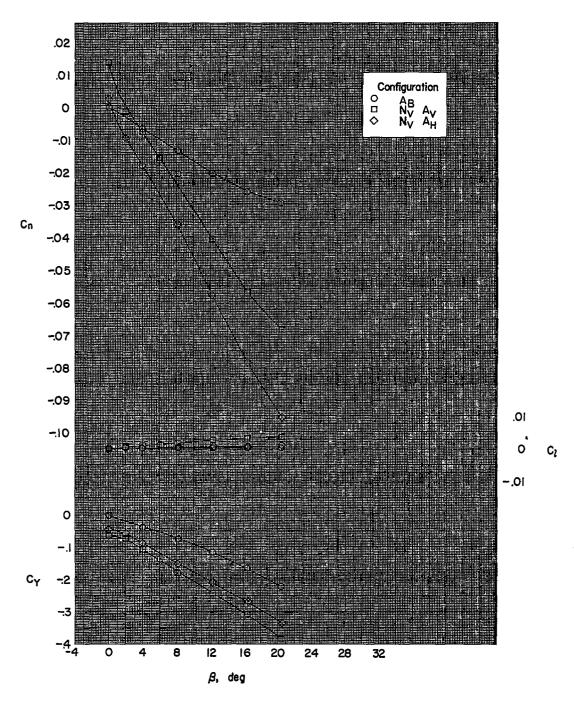(d) $\alpha = 12.2^{\circ}$.

Figure 5.- Continued.
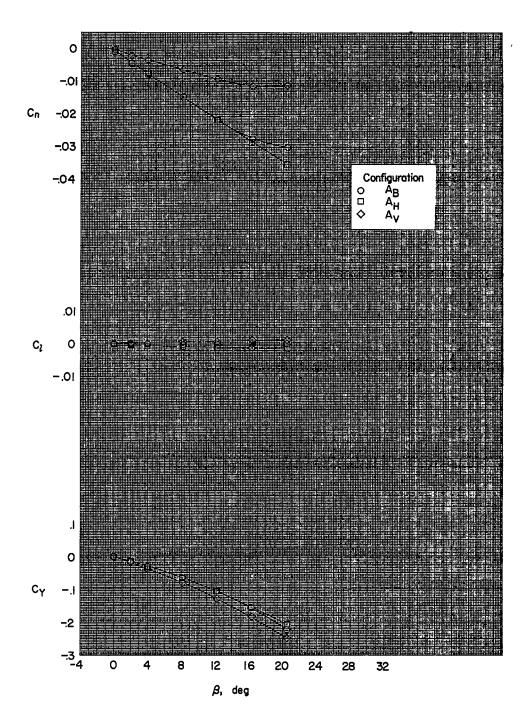
(d) Concluded.
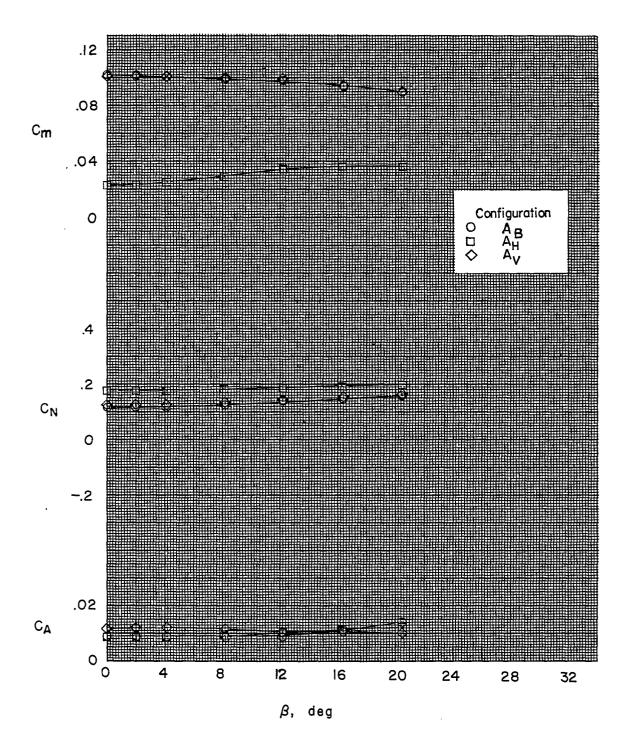
Figure 5.- Continued.

(e) $\alpha = 16.3^\circ$.

Figure 5.- Continued.

Configuration
○ A_B
□ A_H
◇ A_V

β, deg
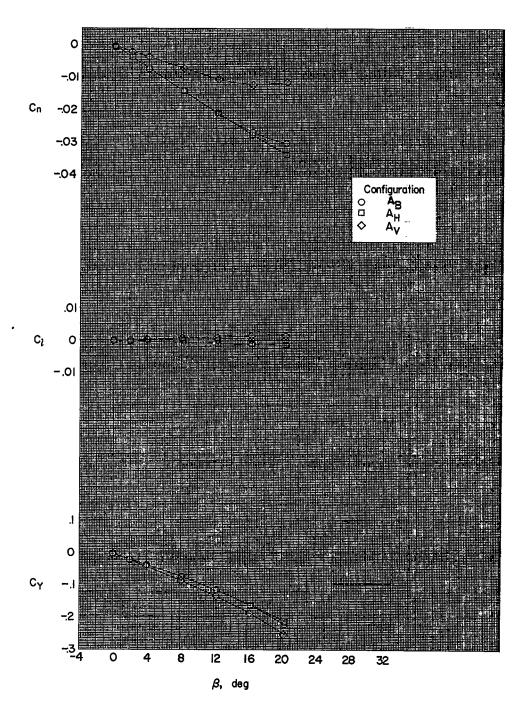
(e) Concluded.
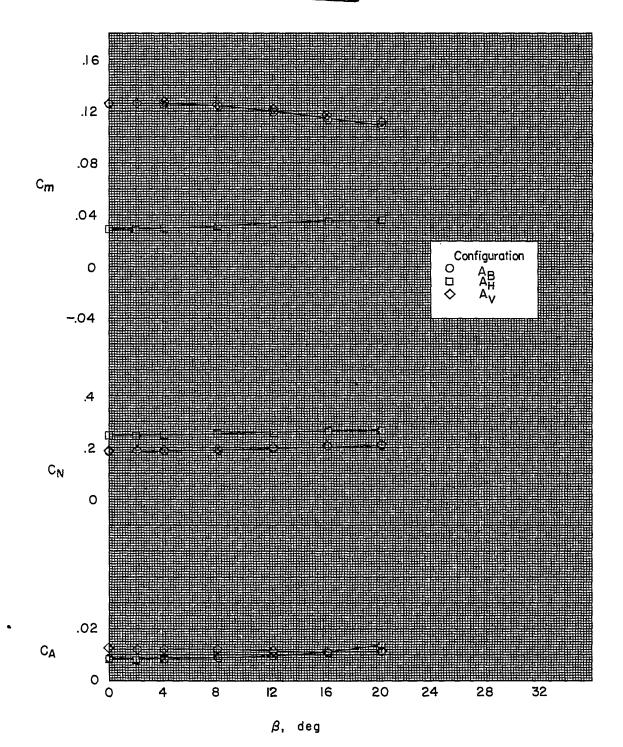
Figure 5.- Continued.

(f) $\alpha = 20.4^{\circ}$.

Figure 5.- Continued.

β, deg
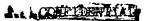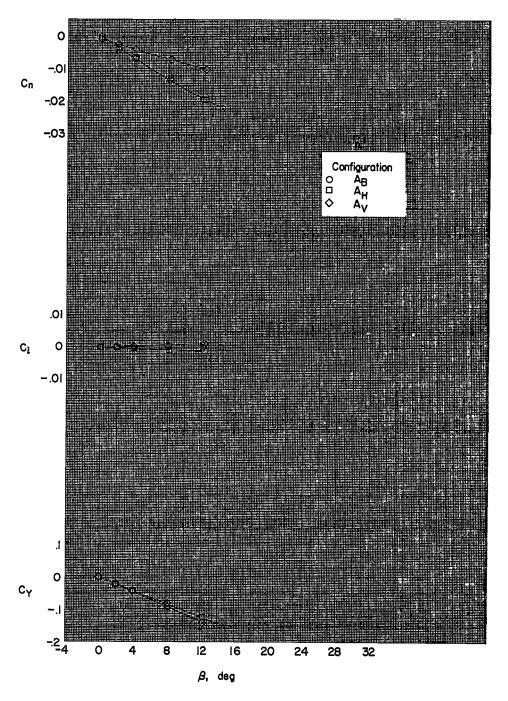
(f) Concluded.
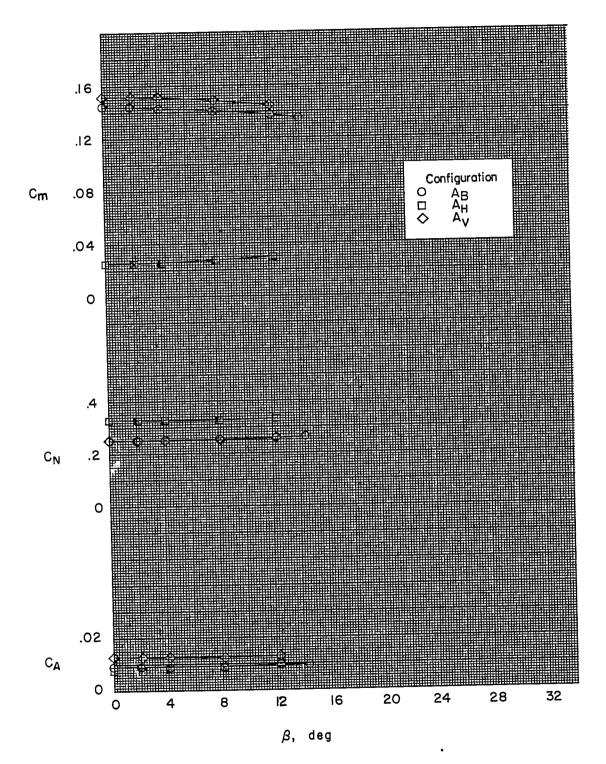
Figure 5.- Continued.

(g) $\alpha = 24.5^\circ$.

Figure 5.- Continued.

(g) Concluded.

Figure 5.- Concluded.

(a) $\alpha = 0^\circ$.
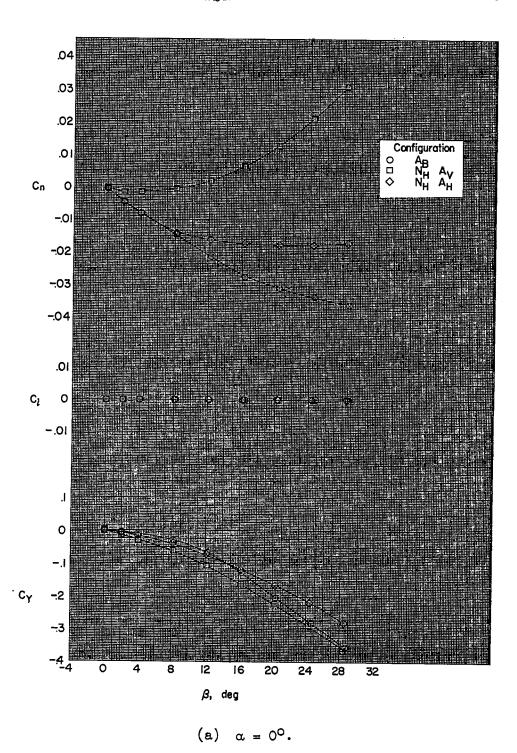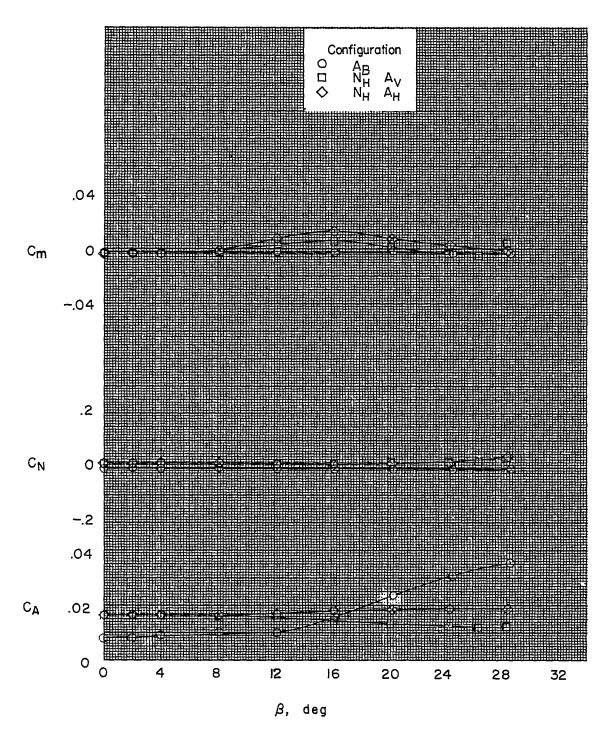
Figure 6.- Aerodynamic characteristics of a body in sideslip with various nose and afterbody configurations. Elliptic nose horizontal.

β, deg
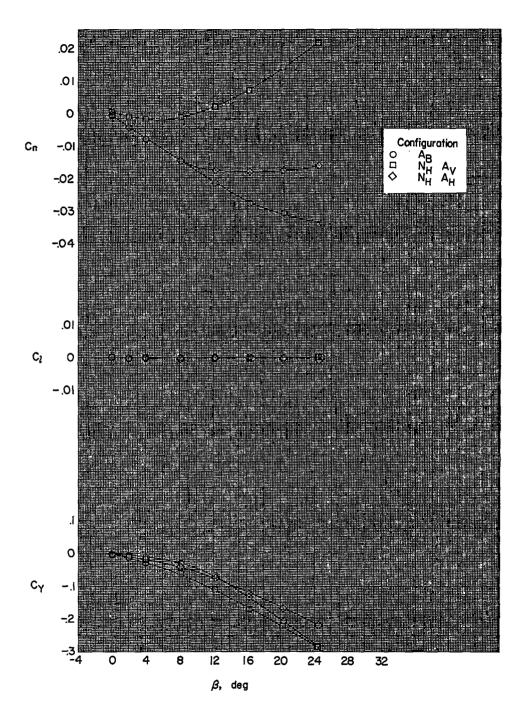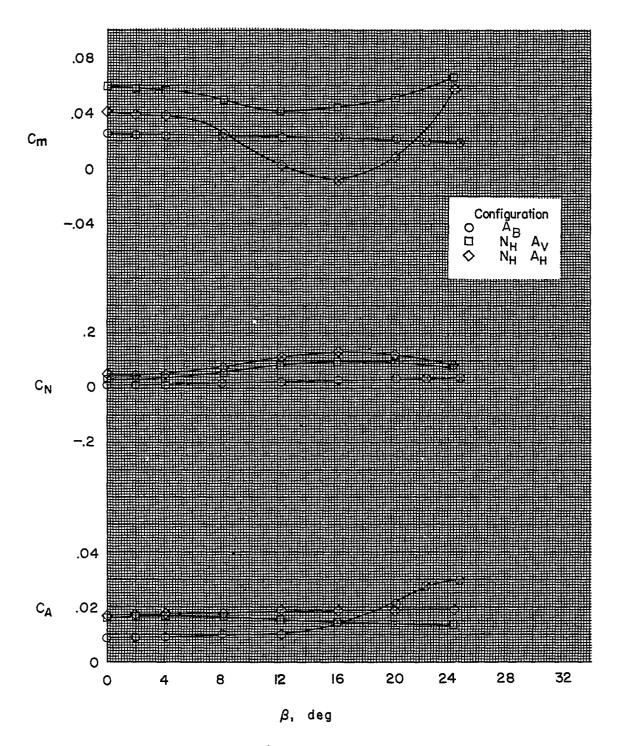
(a) Concluded.

Figure 6.- Continued.

(b) $\alpha = 4.1^\circ$.
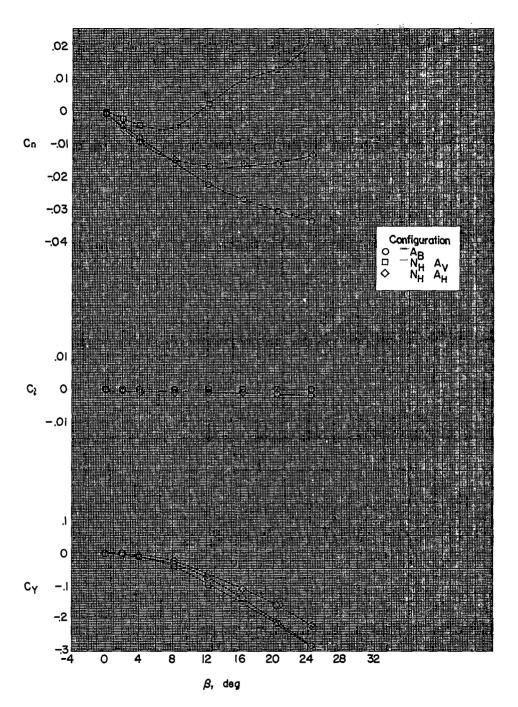
Figure 6.- Continued.

(b) Concluded.
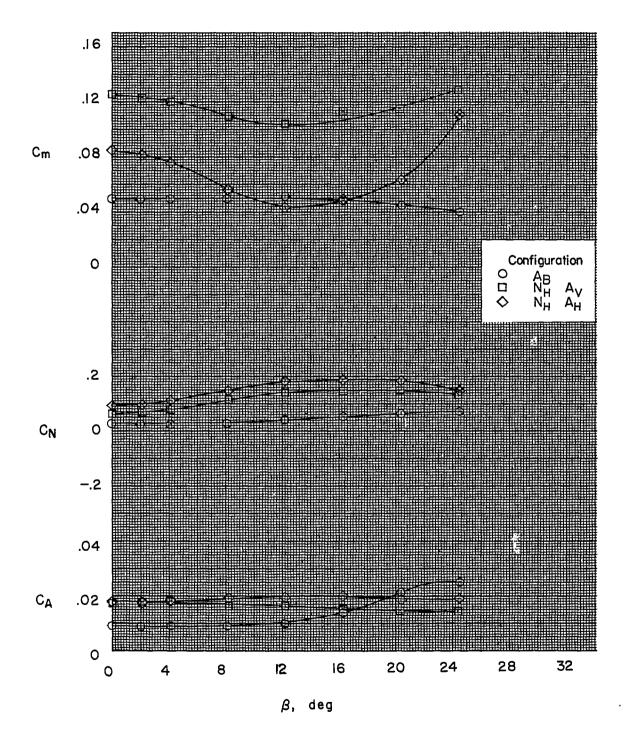
Figure 6.- Continued.

(c) $\alpha = 8.2^{\circ}$.

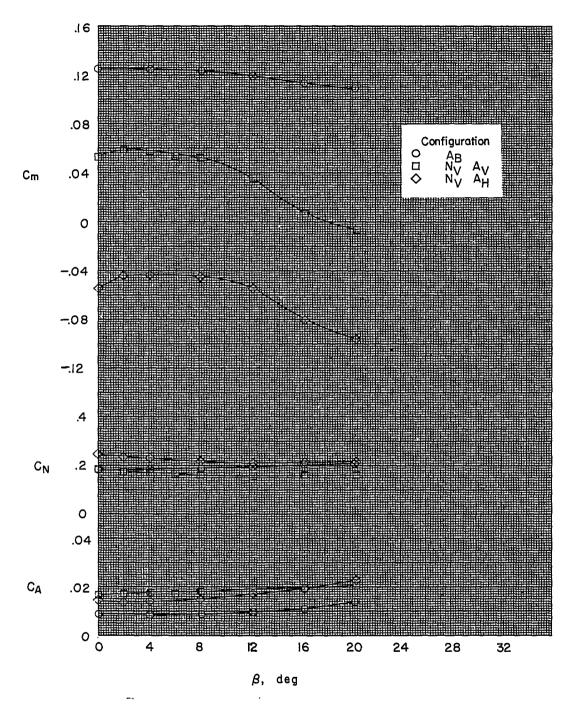Figure 6.- Continued.
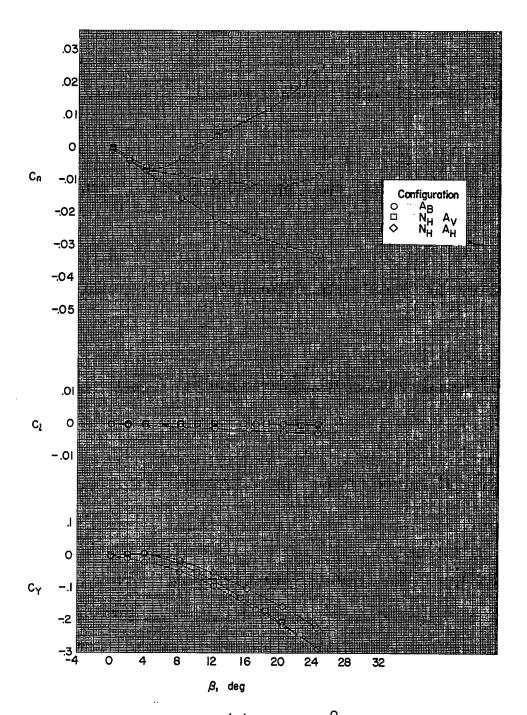
(c) Concluded.
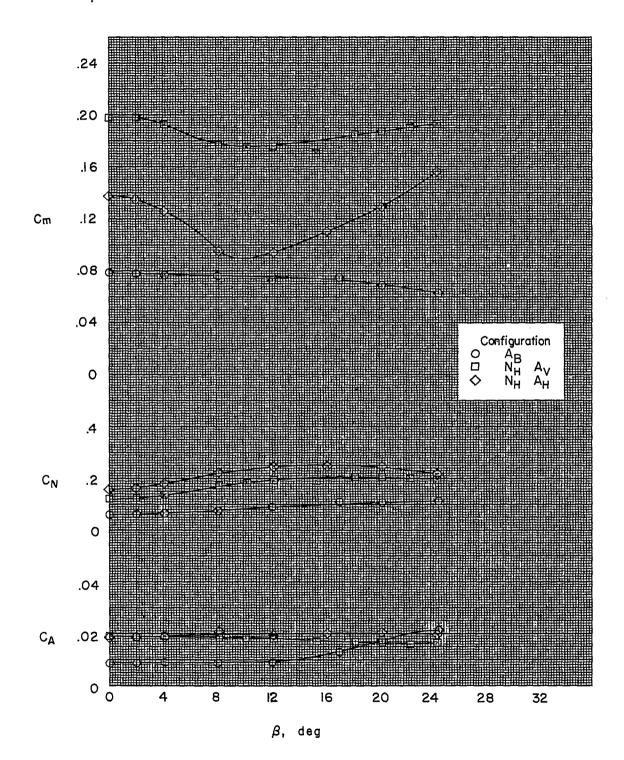
Figure 6.- Continued.

(d) $\alpha = 12.3^{\circ}$.

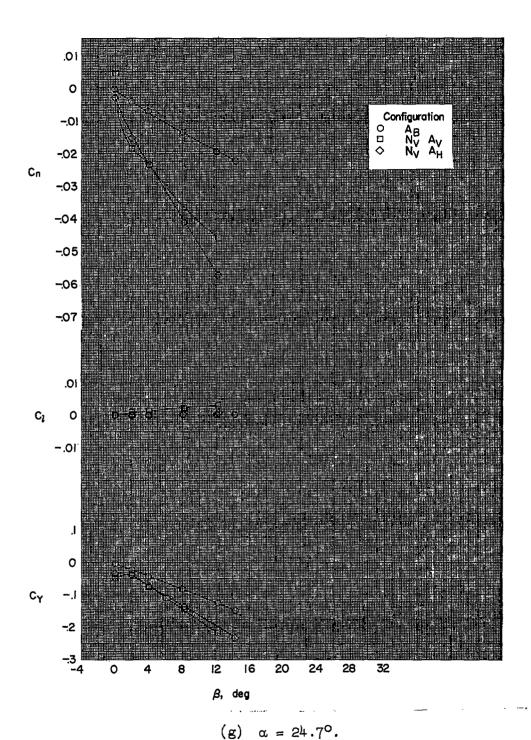Figure 6.- Continued.
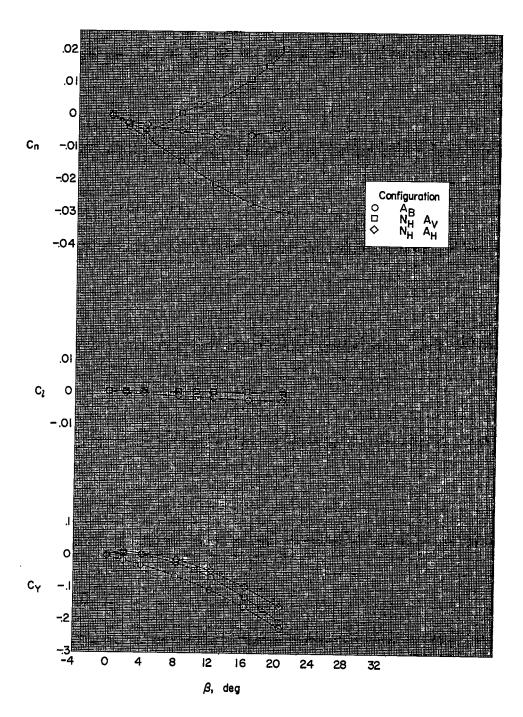
(d) Concluded.
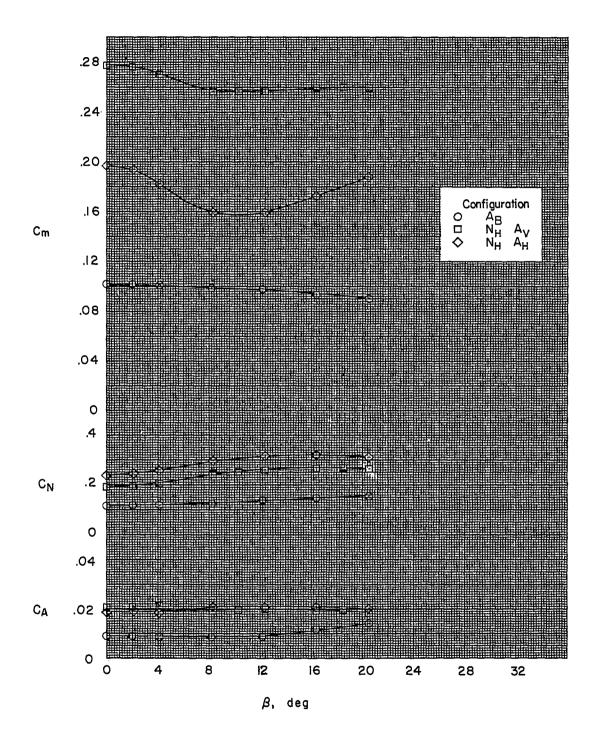
Figure 6.- Continued.
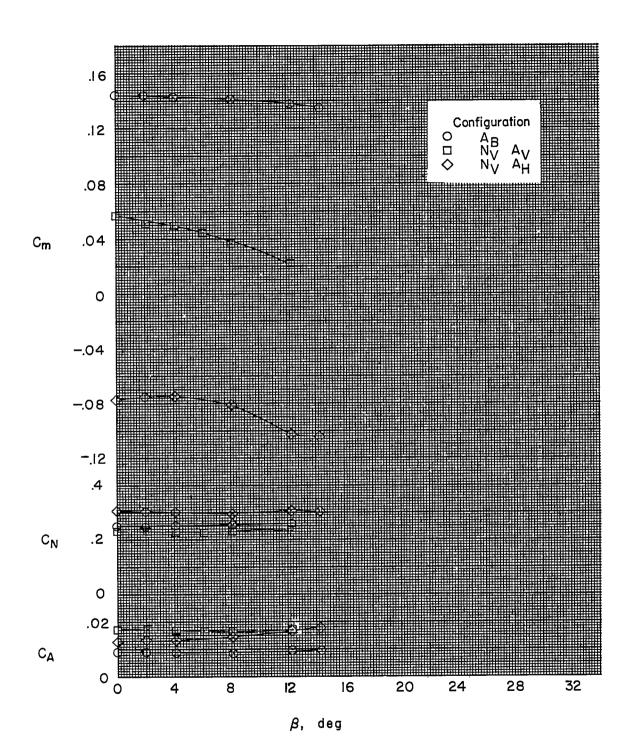
(e) $\alpha = 16.5^{\circ}$.

Figure 6.- Continued.
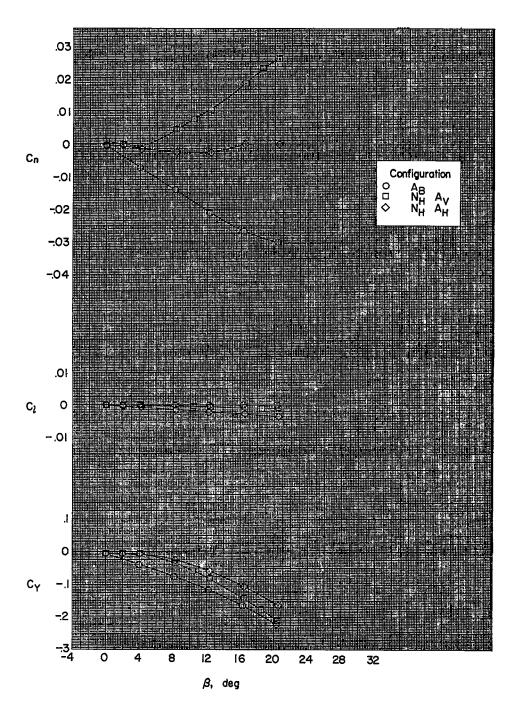
(e) Concluded.
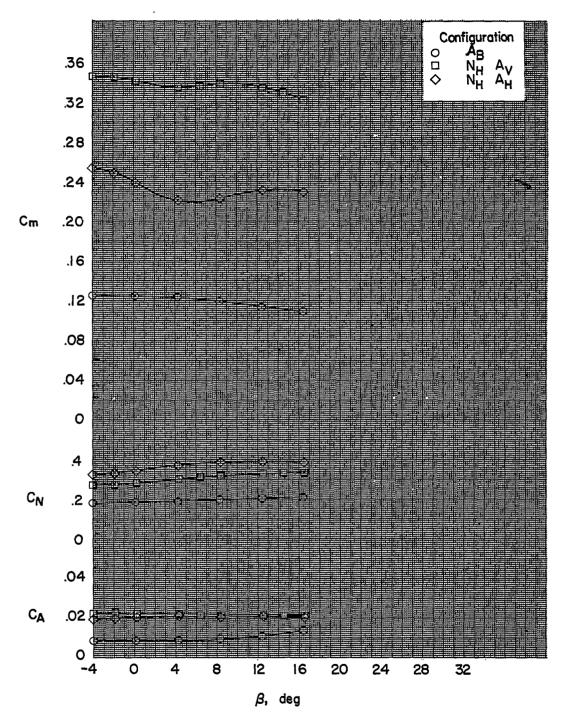
Figure 6.- Continued.

(f) $\alpha = 20.5^{\circ}$.
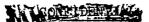
Figure 6.- Continued.
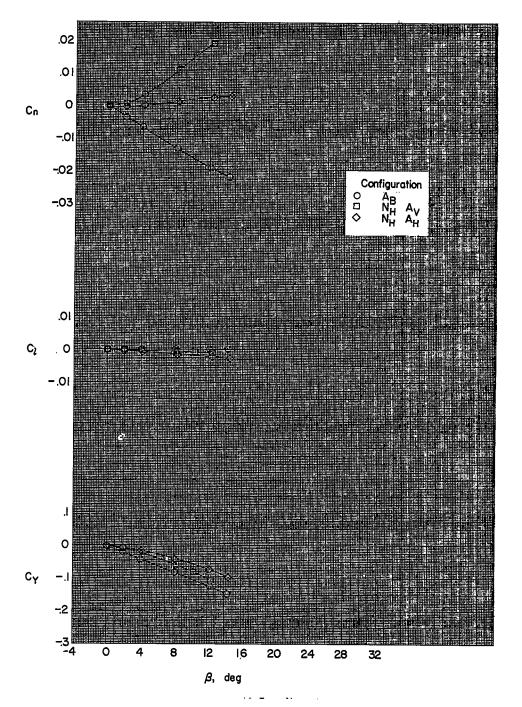
(f) Concluded.

Figure 6.- Continued.

(g) $\alpha = 24.7°$.

Figure 6.- Continued.

(g) Concluded.

Figure 6.- Concluded.

(a) $\alpha = 0°$.

Figure 7.- Aerodynamic characteristics of a body in sideslip with various nose and afterbody configurations. Vertical elliptic nose.

(a) Concluded.

Figure 7.- Continued.

(b) $\alpha = 4.0^{\circ}$.

Figure 7.- Continued.

β, deg

(b) Concluded.

Figure 7.- Continued.

(c) $\alpha = 8.0^o$.

Figure 7.- Continued.

(c) Concluded.

Figure 7.- Continued.

(d) $\alpha = 12.3^{\circ}$.

Figure 7.- Continued.

(d) Concluded.

Figure 7.- Continued.

(e) $\alpha = 16.4^\circ$.

Figure 7.- Continued.

(e) Concluded.

Figure 7.- Continued.

(f) $\alpha = 20.5^{\circ}$.

Figure 7.- Continued.

(f) Concluded.

Figure 7.- Continued.

(g) $\alpha = 24.7^{\circ}$.

Figure 7.- Continued.

(g) Concluded.

Figure 7.- Concluded.
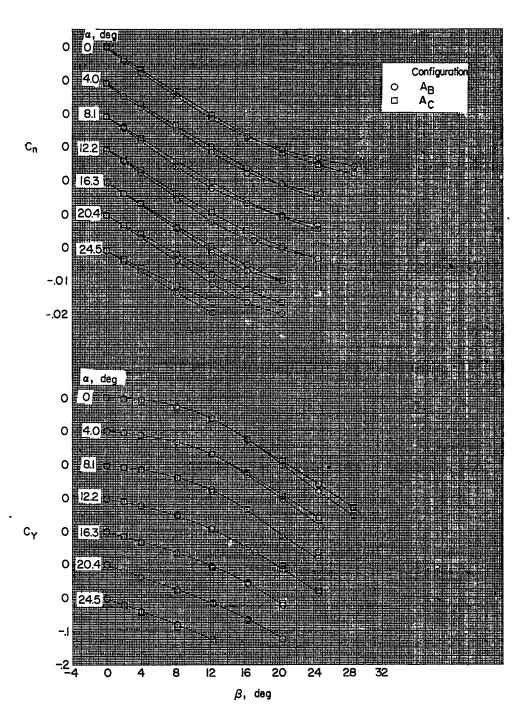
Figure 8.- Comparison of the directional stability characteristics of the boattail and cylindrical afterbody configurations.
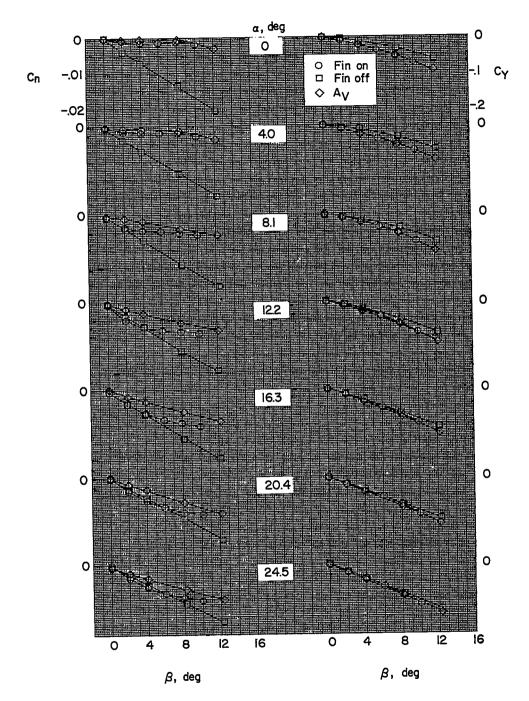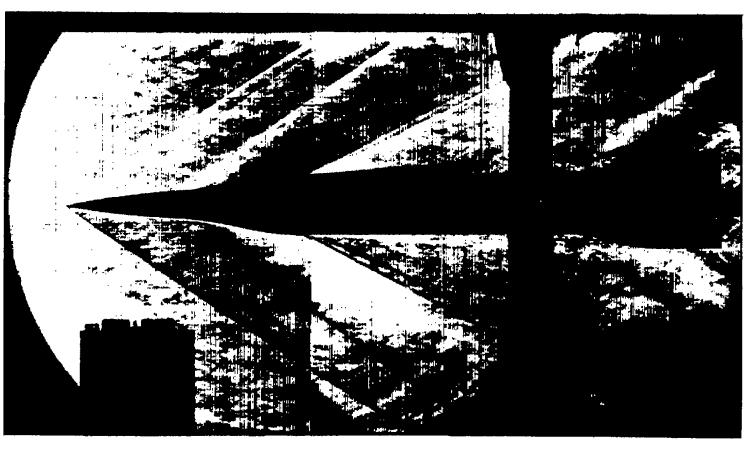
Figure 9.- Comparison of the effect of afterbody fins and vertical
    elliptic afterbody on directional stability characteristics of the
    cylindrical afterbody configurations.
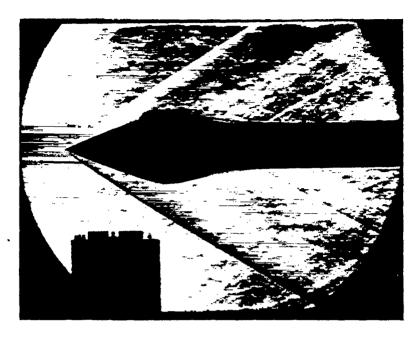
(a) $N_H A_V$; $\alpha = \beta = 0^O$. L-57-4497
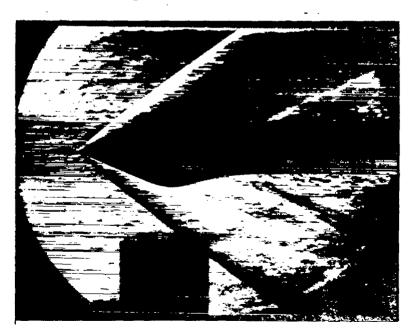
Figure 10.- Schlieren photographs of various body configurations.

(b) N_V; $\alpha = \beta = 0^{\circ}$.   L-57-4498

Figure 10.- Continued.

(c) N_V; $\alpha = 0$; $\beta = 24^{\circ}$.   L-57-4499

Figure 10.- Concluded.

(a) Lateral.
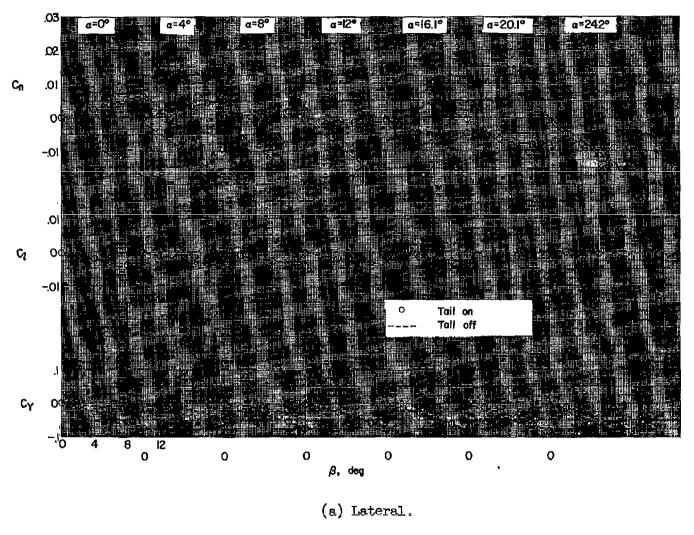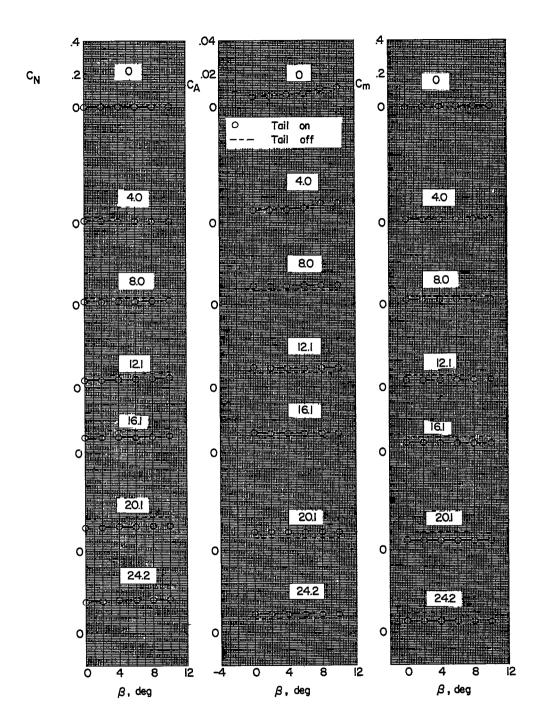
Figure 11.- Aerodynamic characteristics in sideslip of a cylindrical configuration with and without a vertical tail.
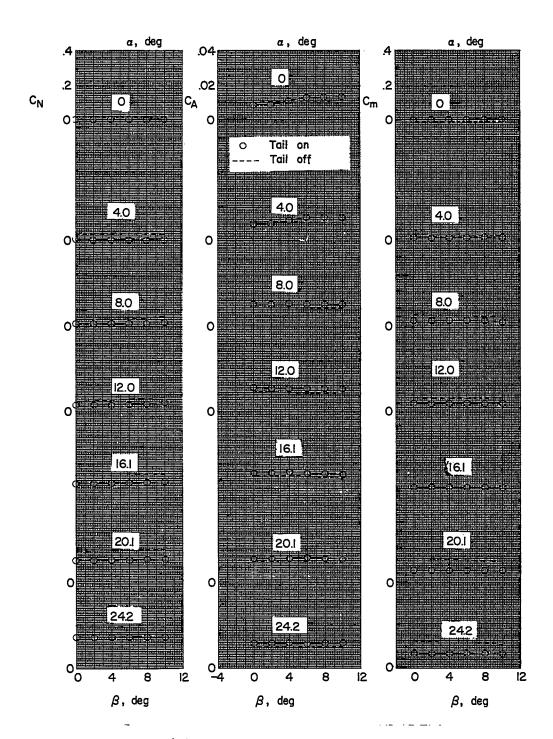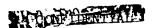
(b) Longitudinal characteristics.

Figure 11.- Concluded.

(a) Lateral.
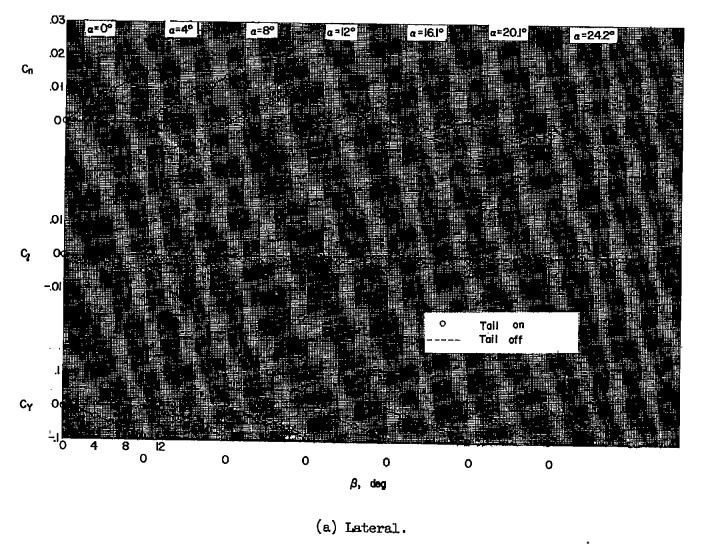
Figure 12.- Aerodynamic characteristics in sideslip of a vertical elliptic-afterbody configuration with and without a vertical tail.

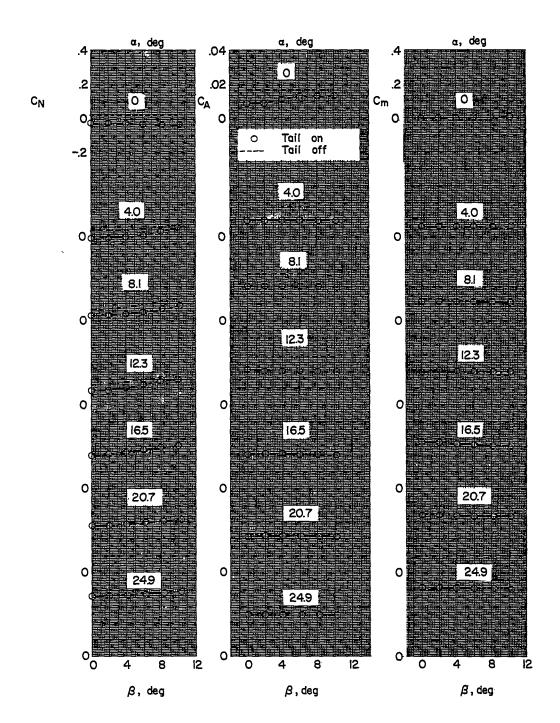(b) Longitudinal characteristics.

Figure 12.- Concluded.

(a) Lateral.

Figure 13.- Aerodynamic characteristics in sideslip of a horizontal elliptic-nose, vertical elliptic-afterbody configuration with and without a vertical tail.

(b) Longitudinal characteristics.
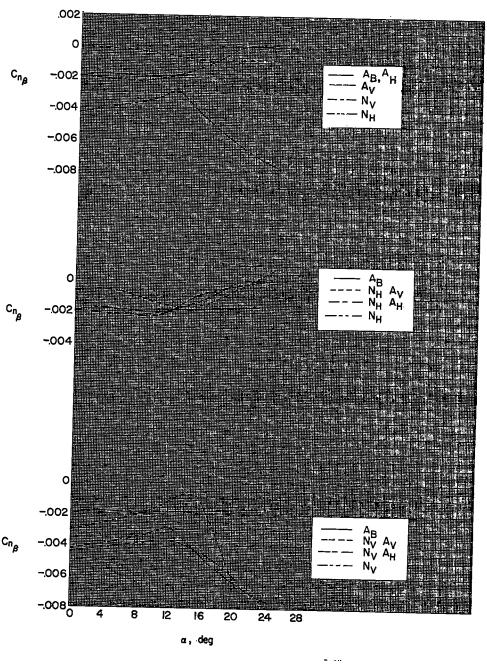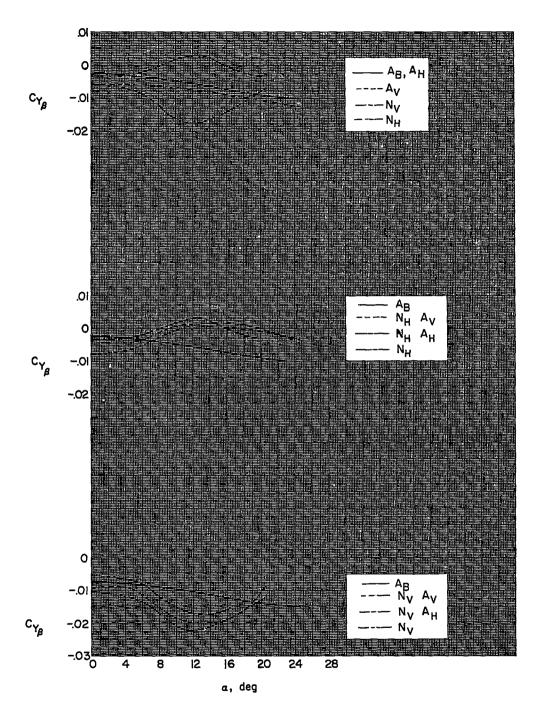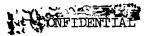
Figure 13.- Concluded.

(a) C_{n_β} against α.

Figure 14.- Effect of various nose and afterbody modifications on the lateral-stability parameters of the bodies alone. $\beta = 0°$.
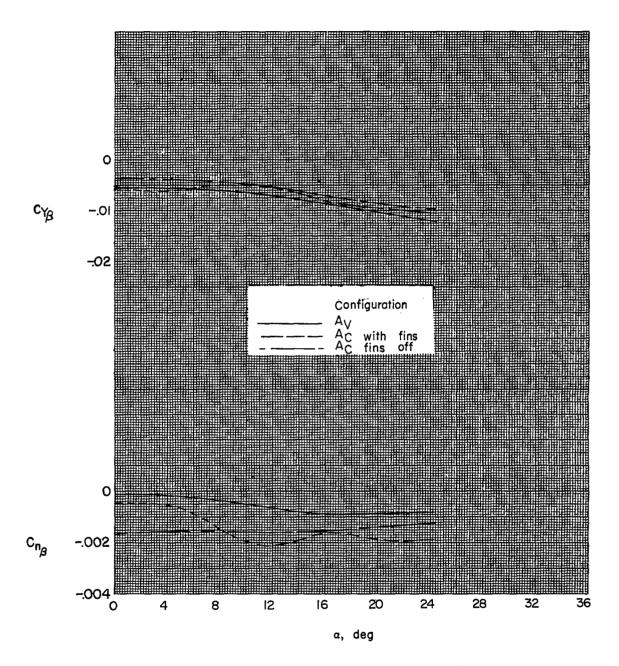
(b) C_{Y_β} against α.

Figure 14.- Concluded.

Figure 15.- Comparison of effect of afterbody fins and vertical ellip-
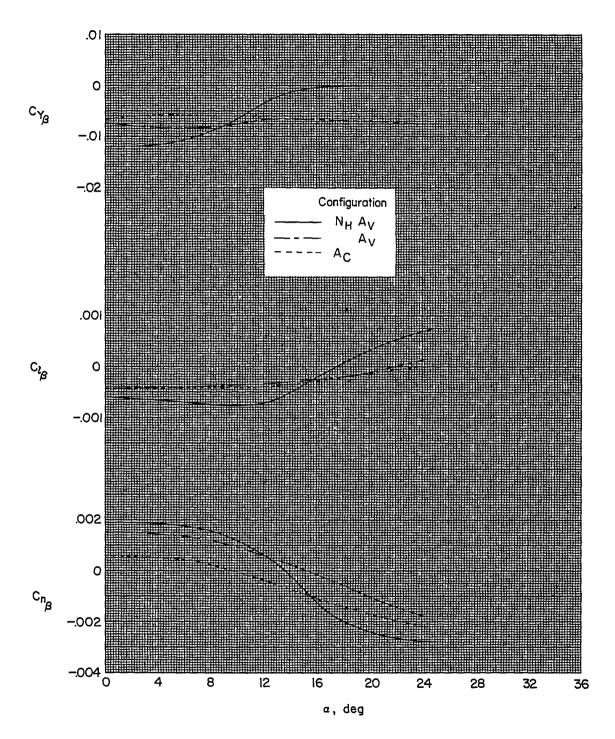tic afterbody on lateral-stability parameters of the body alone.
$\beta = 0°$.

Figure 16.- Effects of a change in nose and afterbody shape on lateral-
stability parameters of the vertical-tail-on configuration. $\beta = 0°$.